Reviews
doi.org/10.1002/batt.202000149

Chemistry Europe
European Chemical Societies Publishing

# Designing Ceramic/Polymer Composite as Highly Ionic Conductive Solid-State Electrolytes

Shangshu Qian,[a] Hao Chen,[a] Zhenzhen Wu,[a] Dongsheng Li,[b] Xianhu Liu,[c] Yongbing Tang,*[d] and Shanqing Zhang*[a]

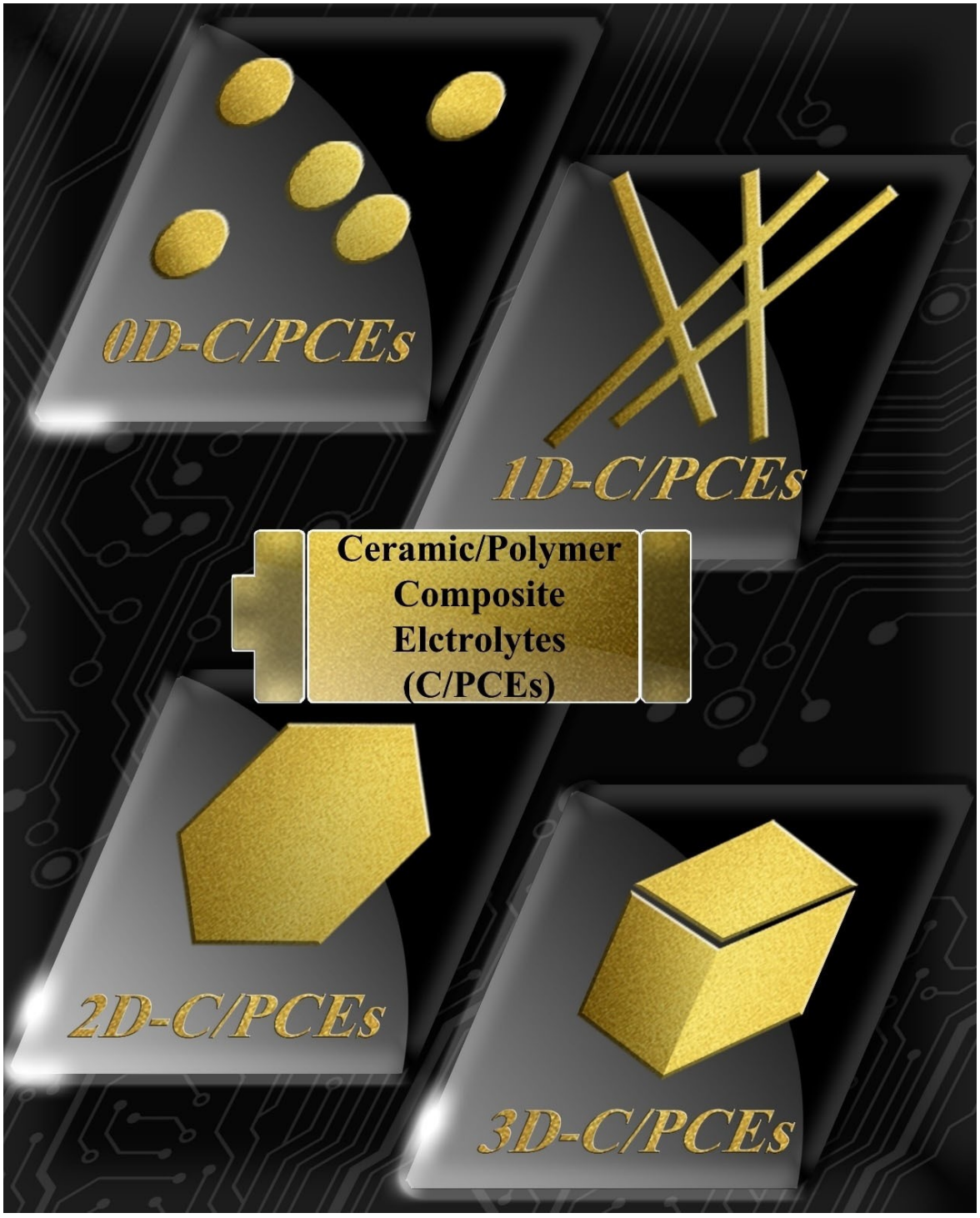

The design and fabrication of solid-state electrolytes (SSEs) with high ionic conductivity is the most crucial obstacle for all-solid-state lithium batteries (ASSLBs). However, though polymer SSEs have the advantages of effective interfacial contact, polymer ASSLBs have not been able to deliver performance comparable to conventional lithium-ion batteries (LIBs) due to slow ion transport within the polymer framework. In contrast, the high inherent ionic conductivity of ceramic SSEs is limited by the poor electrolyte/electrode interfacial contact. Therefore, the concept of ceramic/polymer composite electrolytes (C/PCEs) was proposed to combine the advantages of these two electrolytes and simultaneously overcome their weaknesses. This work reviews the recent progress in C/PCEs development according to the morphology of the ceramic components in C/PCEs. In this review, we investigate the inherent relationship between the structures of C/PCEs and the performance of the resultant SSEs, and subsequently conclude some general C/PCE design principles for future SSEs.

## 1. Introduction

Since the commercialization of lithium-ion batteries (LIBs) in the 1990s, LIBs have considerably changed the daily lives of people. Numerous electronic devices, such as laptops and mobile phones, are becoming more portable and lightweight.[1–3] With the expansion of the automotive application range of LIBs, increasing demands are being made for improved energy density, power density and safety.[4–6] In recent years, the manufacturing technology of electric vehicles (EVs) was gradually matured, leading to rapid growth in the number of EVs worldwide. However, frequent reports of spontaneous combustion of EVs in recent years have generated great resistance to EV development and raised strong concerns about the safety of LIBs.[7,8] In typical traditional LIBs, the liquid electrolyte is the main substance supporting the combustion of LIBs, because its chemical composition is mainly volatile and flammable organic matter.[9,10] Significant improvements and advantages could be brought to LIBs by converting liquid electrolytes to solid polymer or inorganic electrolytes: controllable state, increased safety due to low risk of leakage and volatilization, difficult to burn, higher flexibility. In addition, a wide electrochemical window of SSEs and the application of a lithium anode provide high energy density for ASSLBs.[11]

In general, an ideal SSE needs to meet the following requirements: 1) possess sufficient ionic conductivity at room temperature, at least $10^{-4}$ S cm$^{-1}$; 2) good conductor of lithium ions and an insulator of electrons; 3) a wide electrochemical window; 4) good compatibility with electrode materials; 5) good thermal stability, moisture resistance, and excellent mechanical properties; 6) a simple synthesis method using easily available, low cost raw material. There have been many attempts to identify suitable materials since inorganic or polymer electrolytes were developed in the 1980s and 1990s.[12–14] Currently, inorganic solid electrolytes mainly include perovskite-type (e.g., $Li_{0.5}La_{0.5}TiO_3$ [LLTO]),[15–17] NASICON-type (e.g., $Li_{1.4}Al_{0.4}Ti_{1.6}(PO_4)_3$, [LATP]; $Li_{1.5}Al_{0.5}Ge_{1.5}(PO_4)_3$, [LAGP]),[18–24] and garnet-type (e.g., $Li_7La_3Zr_2O_{12}$, [LLZO])[25–29] in oxides and sulfides (e.g., $Li_{10}GeP_2S_{12}$ [LGPS]).[30–33] Polymer electrolytes mainly include poly(ethylene oxide) (PEO),[34–39] poly(vinylidene fluoride) (PVDF),[40–43] poly(acrylonitrile) (PAN),[44–46] and poly (methyl methacrylate) (PMMA).[47,48]

Unfortunately, there are very few materials that meet all the requirements. Generally, polymer electrolytes, which are easy to process, have significant advantages related to producing intimate interface contact, but the ionic conductivity of polymeric electrolytes is relatively low.[49] Ceramic electrolytes have contrary properties. Sulfide electrolytes possess higher ionic conductivity than other electrolytes, which can reach $10^{-3}$ S cm$^{-1}$ at room temperature. However, sulfide SSEs are unstable in the presence of lithium metal and air. Poor stability is a major obstacle for large-scale application of sulfide electrolytes .[50] In contrast, the good thermal stability of oxide electrolyte makes it easy to process. Furthermore, oxide electrolyte has a sufficiently high ionic conductivity with a lithium-ion transference number close to 1 that can meet the needs of commercial applications. However, poor interfacial compatibility between the oxide electrolyte and the electrode leads to large interfacial resistance.[51,52] Oxide electrolyte and polymer electrolyte can complement each other to a large extent. Much attention has focused on compositing polymer electrolytes with inorganic inert fillers, or modifiers. There have also been many reports on ceramic electrolytes and C/PCEs.[9,11,53,54] However, C/PCEs also have s shortfall. As a composite material, its various properties have no significant defects, however, they also have no outstanding superiority. In actual operation, only one or a few advantages are guaranteed.

The composite of polymer electrolyte and ceramic materials is the focus of this review. Relevant studies in recent years on the structure of ceramic materials are divided into zero-dimensional (0D) composite (particle), one-dimensional (1D) composite (nanowire or nanowire network), two-dimensional (2D) composite (layered structure) and three-dimensional (3D) composite (Figure 1). The following section will summarize these different structures, their properties and uses and discuss

[a] S. Qian, H. Chen, Z. Wu, Prof. S. Zhang
Center for Clean Environment and Energy,
School of Environment and Science,
Griffith University, Queensland 4222, Australia
E-mail: s.zhang@griffith.edu.au
[b] Prof. D. Li
College of Materials and Chemical Engineering,
Key Laboratory of Inorganic Nonmetallic Crystalline and
Energy Conversion Materials,
China Three Gorges University, Yichang, 443002, China
[c] Dr. X. Liu
Key Laboratory of Materials Processing and Mold
Zhengzhou University,
Ministry of Education, Zhengzhou, P.R. China
[d] Prof. Y. Tang
Shenzhen Institutes of Advanced Technology,
Chinese Academy of Sciences, Shenzhen 518055, China
E-mail: tangyb@siat.ac.cn

the mechanism of lithium-ion conduction of the composite structure.

### 1.1. State-of-the-Art Polymeric Solid-State Electrolyte

A variety of polymers, such as PEO,[55,56] PVDF,[57,58] PAN,[59,60] Poly (ethyl carbonate) (PEC),[61,62] poly(propyl carbonate) (PPC),[63,64] and PMMA,[47] have been investigated as polymer materials. Among them, the most common is PEO. PEO is a polyether. The chain composed of the structural unit of –($CH_2$–$CH_2$–O)– possesses high flexibility and can be used for lithium-ion conduction. Moreover, PEO has excellent lithium-salt solubility. These advantages make PEO the most promising polymer electrolyte for commercial application today.[65] Generally, the lithium-ion conductivity of a commercial battery electrolyte is required to be at least $10^{-3}$ S cm$^{-1}$ at room temperature. Unfortunately, the lithium-ion conductivity of PEO mixed with lithium-salt at room temperature is only about $10^{-7}$–$10^{-6}$ S cm$^{-1}$. The low lithium-ion conductivity is primarily due to the coexistence of crystalline and amorphous phases in the PEO and lithium salt mixture.[66] Moreover, it is believed that the ionic conductivity of PEO is mainly due to the contribution of amorphous PEO, while crystalline PEO hinders the transport of lithium ions. Therefore, reducing the crystalline phase and increasing the amorphous content are the main strategies to improve the lithium-ion transport performance of PEO. The common methods to reduce the crystallinity of PEO are adding inorganic modifiers,[67–70] adding plasticizers,[71,72] and forming copolymers[73,74] with other polymers. Adding inorganic modifiers can be divided into adding inert and active modifiers. For instance, Pitawala et al. investigated the improvement effect of adding $Al_2O_3$ as an inert modifier and ethylene carbonate (EC) as plasticizers on the ionic conductivity of $(PEO)_9LiTf$ electrolyte and the combined effect of EC and $Al_2O_3$ on $(PEO)_9LiTf$. $Al_2O_3$ better enhanced the crystalline phase (below 55 °C), and the addition of 15 Wt.% increased the ionic conductivity of $(PEO)_9LiTf$ to $2.1\times10^{-5}$ S cm$^{-1}$ at room temperature (25 °C).[75]

Shangshu Qian received his bachelor's and master's degrees in chemistry from Ningbo University (China) in 2015 and 2018, respectively. Now he studies for his doctorate degree at Griffith University, under the guidance of Professor Shanqing Zhang. His main research interests are developing novel polymer-based electrolytes and their composites with ceramic-based electrolytes for solid-state batteries.

Hao Chen was awarded his bachelor's and master's degrees in chemistry from Central South University (China) in 2014 and 2017, respectively. Since 2017, he has been a chemistry Ph.D. student at the School of Environment and Science, Griffith University, Australia. His current research interests include the design and synthesis of functional binders, and solid-state electrolyte for all-solid-state lithium-ion batteries and lithium–sulfur batteries.

Zhenzhen Wu is a Ph.D. candidate under the supervision of Prof. Shanqing Zhang in Griffith University (Australia). She received her B.Eng. and M.S. degree at Jiangsu Normal University and Nankai University (China) in 2014 and 2017, respectively. Her current research mainly focuses on organic electrode materials, MOFs, and nanomaterials for rechargeable secondary batteries.

Prof. Dong-sheng Li received his Ph.D. in chemistry from Northwest University of China in 2005 under the supervision of Prof. Yao-Yu Wang. He became a professor in 2005 and joined China Three Gorges University in 2008. His interests focus on the design of novel MOFs and nanomaterials for energy and environmental applications.

Xianhu Liu is currently an associate professor at the National Engineering Research Center for Advanced Polymer Processing Technology in Zhengzhou University, China. He received his Ph.D. degrees respectively from Zhengzhou University in Henan, China, and Friedrich-Alexander-University Erlangen-Nuremberg in Erlangen, Germany. His most recent interests concern the development of new polymer processing technology, polymer rheology and processing, preparation of advanced polymer composites as well as polymer porous materials.

Prof. Yongbing Tang received his Ph.D. degree from the Institute of Metal Research (IMR), CAS in 2007 with Prof. Hui-Ming Cheng. He was a Research Fellow at the City University Hong Kong (2007–2013). He is currently a professor and Director of Functional Thin Films Research Center at Shenzhen Institutes of Advanced Technology, Chinese Academy of Science, China. His research mainly focuses on energy storage materials and devices.

Prof. Shanqing Zhang obtained his Ph.D. degree in electrochemistry in 2001 at Griffith University, Australia. As a core inventor, Prof. Zhang has developed a series of patented and commercialized technologies for environmental monitoring and energy storage devices based on functional nanomaterials. He was awarded the Australia Research Council Future Fellowship for 2009–2013 and promoted as a full professor and theme leader in Griffith University since 2016. Currently, Prof. Zhang has been working on design and synthesis of nanomaterials and functional polymers for energy conversion and storage devices as well as the development of sustainable recyclable battery technology.

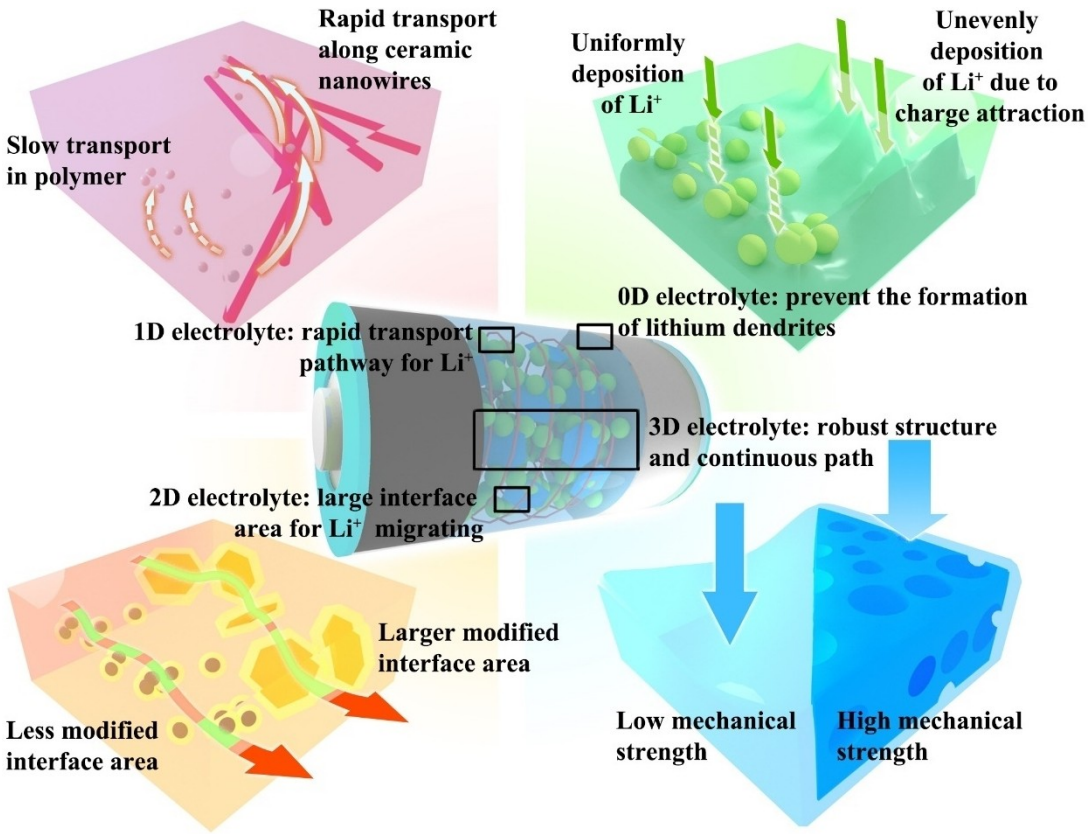


**Figure 1.** Schematic diagram of a) 0D, b) 1D, c) 2D, and d) 3D ceramic/polymer composite electrolytes (C/PCEs) and their main advantages.

Choi et al. evaluated the performance of PEO electrolytes with different tetragonal $Li_7La_3Zr_2O_{12}$ content. They found that the 52.5% LLZO sample exhibited the highest ionic conductivity of $4.42\times10^{-4}$ S cm$^{-1}$ at 55 °C. A sample with 52.5% $Al_2O_3$ was tested in comparison to the 52.5% LLZO sample, the ionic conductivity of the former is an order of magnitude lower than that of the latter.[76]

The structural unit of PAN has a strong electron-withdrawing nitrile group (C≡N), which differs from the –($CH_2$–$CH_2$–O)– group of PEO. Therefore, the lithium-ion transport mechanism of PAN differs to that of PEO. In addition, PAN is basically an amorphous phase, and chain activity contributes little to ionic conductivity. Therefore, PAN is widely used as a matrix to accommodate liquid electrolyte to prepare gel electrolytes. It is an excellent electrolyte choice due to its high ionic conductivity, wide electrochemical window, and excellent chemical stability attributed to the presence of a nitrile group.[77] However, the mechanical strength of PAN is relatively low, so it is generally necessary to add modifiers to enhance strength. Currently, the reported ionic conductivity of PAN with inorganic modifiers is generally in the order of $10^{-4}$ S cm$^{-1}$.[78,79]

The structural unit –(CH–CF)–, of PVDF contains a stronger electron-withdrawing functional group –CF- than PAN, which is conducive to the dissolution of lithium salts and stability to lithium metal anode.[9,80] For applications involving gel electrolytes, hexafluoropropylene (HFP) is added into PVDF to form the copolymer PVDF-HFP with lower crystallinity as the amorphous phase can absorb a large amount of liquid electrolyte.[81] There is a drawback of using PVDF with lithium metal anodes as fluorine will react with lithium to form lithium fluoride. However, lithium fluoride could potentially improve the cycling stability of lithium metal batteries.[82] Therefore, some works even purposely introduce LiF between the lithium metal and solid electrolyte to improve the cycling stability of lithium metal batteries.[82,83]

There is a typical electron-donating functional methoxycarbonyl group (–$COOCH_3$) in the structural unit of PMMA, which indicates that PMMA can coordinate well with lithium ions. Therefore, PMMA has a similar lithium-ion transport mechanism to PEO. The conductivity of lithium ions depends largely on the selection of lithium salt and the segment motion of the PMMA chain. Many studies have examined the lithium salt system used in PMMA. According to the different lithium salt and plasticizer used, the lithium-ion conductivity of PMMA based electrolytes can vary significantly ($10^{-6}$ to $10^{-4}$ S cm$^{-1}$).[47,84–86]

PEC and PPC are both polycarbonates (PC). Similar to PEO and PMMA, there is a considerably strong electron-donating functional carbonate group (–OCOO–) in PC for coordinating with lithium ions. The advantages of PC electrolytes are high lithium-ion conductivity, stability to lithium metal anode, and wide electrochemical window. Furthermore, unlike PEO, PC possesses a high lithium ion transference number.[87] The disadvantage of PC is a common problem with most polymer

electrolytes, low mechanical properties, requiring an inorganic modifier to improve performance.[88]

#### 1.1.1. Li–Ion Transport Mechanism in Polymeric Solid-State Electrolyte

As described above, most polymer electrolytes rely on the coordination of electron-donating groups and lithium ions to transport lithium ions. In the case of PEO, the oxygen atom in the backbone is the electron-donating group used to coordinate with lithium ions (Figure 2). During the lithium-ion transport process, the lithium-ion first coordinates with several oxygen atoms. With the chain segment oscillating, the lithium-ion is delivered to another uncoordinated oxygen on the same chain or another chain. By repeating this process, lithium ions can be transported through the PEO electrolyte.

Although PEO has good ionic conductivity, it is not entirely attributed to the transport of lithium ions. The anions produced by the decomposition of lithium salts also migrate under the action of the electric field and provide partial ionic conductivity. Therefore, the concept of ion transference number is involved. The ion transference number generally refers to the proportion of the mobility of a certain part of the total mobility. Taking the electrolyte of a single lithium salt as an example, the lithium-ion transference number is the ratio of the mobility of the lithium-ion to the sum of the mobility of the lithium-ion and anion (Equation (1), $t^+$ is the cation transference number, and $\mu^+$ and $\mu^-$ are cation mobility and anion mobility, respectively).[89]

$$t^+ = \frac{\mu^+}{\mu^+ + \mu^-} \tag{1}$$

The power density and energy density of LIBs can be improved by increasing the lithium-ion transference number. Current approaches involve fixing the anion to avoid anion migration, thereby increasing the lithium-ion transference number.

#### 1.1.2. Application and Challenges

Polymers can be used in various electrochemical devices, such as electrochemical capacitors, due to their "semi-solid and semi-liquid" state. In commercialized electrical double-layer capacitors, both aqueous and non-aqueous electrolytes are liquid, which has a great risk of leakage. Using polymer electrolyte as a substitute not only eliminates this risk and achieves long-term stability, but also has the advantages of a wide temperature operating window and flexibility. The same is true in battery systems. The polymer electrolyte can effectively avoid the risk of electrolyte leakage, but its shortfalls cannot be ignored. The properties of polymeric electrolytes vary significantly depending on the temperature. At low temperatures, the lithium-ion conductivity of polymeric electrolytes is generally low. Even with the lowest application standard ($10^{-4}$ S cm$^{-1}$), there is an order of magnitude gap. As the temperature increases, the lithium-ion conductivity of the polymeric electrolyte improves markedly, but the mechanical strength decreases. Therefore, the development of polymeric electrolytes capable of achieving high ionic conductivity at room temperature and maintaining mechanical strength is currently a major challenge.

### 1.2. Ceramic Solid-State Electrolyte

Currently, the most widely studied inorganic SSEs are divided into oxide (perovskite-type, NASICON-type, and garnet type) and sulfide types. Sulfur atoms have a larger atomic radius than oxygen atoms, which provides a larger transport path for lithium ions. The binding energy of lithium-ion and sulfur ion is low, which makes it easier for the lithium-ion to migrate. Due to excellent ductility and fluidity, sulfides have higher ionic conductivity than oxides, even comparable to liquid electrolytes.[50] However, sulfides are rarely used in C/PCEs due to their poor thermal stability.

Perovskite-type ceramic electrolytes were firstly reported in 1971,[90] which generally have the chemical formula $ABO_3$. One of the most typical of this type of electrolyte is $Li_{3x}La_{2/3-x}TiO_3$

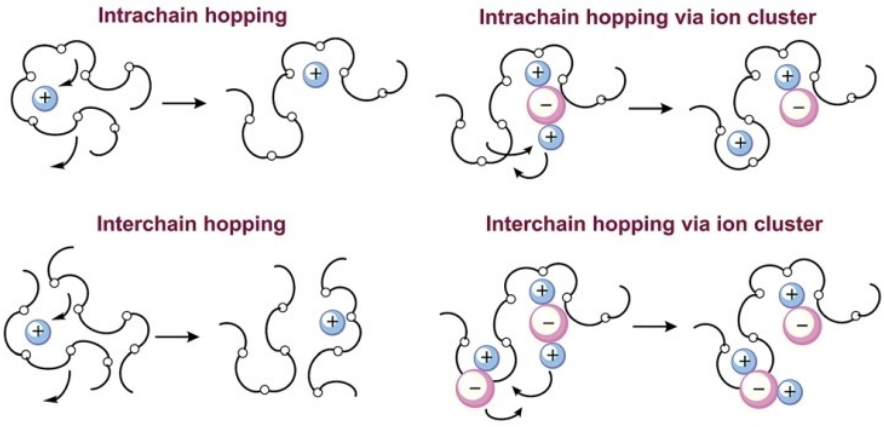


**Figure 2.** Mechanism of ion transport in PEO.[65] Reproduced with permission from Ref. [65]. Copyright (2015) Royal Society of Chemistry.

(LLTO). The LLTO crystal frame is mainly composed of $TiO_6$ octahedra, and both $Li^+$ and $La^+$ occupy the A site. Since lithium ions mainly move through channels formed by the vacancies in A sites, ions with a large ion radius, such as lanthanum ion, can provide wider channels for lithium-ion migration.[91] As an electrolyte for SSBs, LLTO has a high ionic conductivity of $10^{-3}$ S cm$^{-1}$ at room temperature. However, it should be noted that this high ionic conductivity is delivered from a single crystal. Only $10^{-5}$ S cm$^{-1}$ can be produced at room temperature by polycrystals due to barriers to lithium-ion transport caused by grain boundaries.[92] Therefore, reducing the grain boundaries in the LLTO membrane is an efficient strategy for practical application. Another problem is that LLTO is unstable when in contact with Li metal anode since $Ti^{4+}$ will be reduced to $Ti^{3+}$ when the potential is below 1.8 V vs. $Li^+$/Li.[93] Adding a buffer layer between the LLTO and the lithium metal anode may be effective, and may also improve the contact between the two.

The Na Super-ionic Conductor (NASICON) can be used to transport sodium ions. Extensive research on NASICON materials began when Goodenough et al. first proposed the NASICON SSE $Na_3Zr_2Si_2PO_{12}$ in 1976.[94] NASICON material has an open 3D sodium-ion transport channel. After replacing sodium with lithium, the structure can be used as an excellent lithium-ion transport medium. To increase the ionic conductivity, Al is added to the structure. Two representative NASICON-type ceramic electrolytes are LATP and LAGP, and their ionic conductivity can reach $10^{-3}$ and $10^{-4}$ S cm$^{-1}$, respectively.[95,96] While the ionic conductivity of LATP is higher than LAGP, LATP can react with lithium metal anodes under 2.4 V vs. $Li^+$/Li, which is similar to LLTO.[96] As with LLTO, this problem can also be solved by adding a buffer layer between LATP and the lithium metal anode. LATP, and LAGP exhibit high electrochemical stability at high voltage, which is their most prominent advantage as SSEs.

Garnet-type LLZO is a representative of garnet-type SSEs. As mentioned above, LATP and LLTO have a common disadvantage of reacting with the lithium metal anode below a certain potential (2.4 or 1.8 V vs. $Li^+$/Li). In contrast, LLZO possesses excellent stability on the lithium metal anode due to its low reduction potential (-3.05 V). LLZO can achieve high ionic conductivity ($1.2\times10^{-2}$ S cm$^{-1}$ at room temperature), basically equivalent to sulfide, and is more stable in air than sulfide.[97] Although LLZO reacts with moisture in the air, these carbonate layers can be removed by simple means. Therefore, the stability of LLZO is undoubtedly a significant advantage in its application. The poor contact on the electrode-electrolyte interface and resistant ability to lithium dendrite penetration are the main problems of LLZO. Hu et al. inserted thin $Al_2O_3$[98] and Li–Al alloy[99] layers between the lithium metal anode and a $Li_7La_{2.75}Ca_{0.25}Zr_{1.75}Nb_{0.25}O_{12}$ (LLCZN, garnet-type) layer. Both means can effectively improve wettability and reduce the interfacial resistance. However, the high interfacial resistance is not due to LLZO itself. According to the work of Sharafi et al., $Li_2CO_3$ and LiOH layers on the surface of LLZO lead to the high interfacial resistance. After removing the carbonate layer, LLZO shows great wettability to Li and the interfacial resistance can be reduced to 2 Ω cm$^2$,[100] which provides a different way to resolve the problem.

Sulfides are also a crucial electrolyte material. Sulfides are generally including Li-P–S-based glasses and glass ceramics, $Li_6PS_5X$ (X=Cl, Br, or I) argyrodites, thio-LISICONs and $Li_{11-x}M_{2-x}P_{1+x}S_{12}$ (M=Ge, Sn, and Si) compounds.[50] Among these materials, $Li_{9.54}Si_{1.74}P_{1.44}S_{11.7}C_{10.3}$ has the highest ionic conductivity of $2.5\times10^{-2}$ S cm$^{-1}$ at room temperature,[101] which is comparable to liquid electrolyte. However, its poor electrochemical and chemical stability limit its application in the batteries with high working voltage cathode or lithium metal anode. For example, the typical sulfide LGPS was calculated that the real electrochemical window is 1.7–2.1 V.[102] According to the work, LGPS is lithiated into $Li_4GeS_4$, P, and $Li_2S$ at 1.7 V, And delithiated into $Li_3PS_4$, S, and $GeS_2$ at 2.14 V. It can enlarge the electrochemical window to a certain extent by controlling synthesis parameters and the consequent microstructural compositions.[103] In addition, LGPS can react not only with lithium metal to form $Li_2S$, $Li_3P$, and LiCl,[104] but also with cathode oxides like $LiCoO_2$. The introduction of an intermediate layer to block the contact of sulfide with the anodes or cathodes can reduce the occurrence of these reactions.[50]

### *1.2.1. Mechanism of Li–Ions Transport in Ceramic Solid-State Electrolyte*

Driven by an electric field gradient, lithium ions contained in SSEs or foreign lithium ions can travel through the solid. There are several common mechanisms of lithium-ion transportation: direct interstitial mechanism, vacancy mechanism, interstitialcy mechanism, interstitial-substitutional exchange mechanism (dissociative mechanism and knock-off mechanism), and collective mechanism, as shown in Figure 3. The direct interstitial mechanism means lithium ions diffuse in the interstitialcy between the skeletons of molecules. The interstitialcy should be larger than the lithium-ion radius. For example, there are a large number of interstitials in the interstitial solid solution, which are much more abundant than the interstitial atoms, so the interstitial atoms can be rapidly diffused. The direct interstitial mechanism is the most fundamental type. The vacancy mechanism refers to the transport of ions by jumping to the adjacent vacancy. Since the hopped ions will generate new vacancies in the original position, ion transport can follow this cycle. As lithium-ion transport depends on vacancies, means of increasing the ratio of vacancies, such as doping with different valence ions, can greatly enhance the ionic conductivity. However, in practical cases, the transport of lithium ions may be more complex, such as the participation of multiple ions (the interstitialcy mechanism and collective mechanism) or a combination of multiple mechanisms (interstitial-substitutional exchange mechanism).

LLTO has many different crystal structures, such as cubic, hexagonal, tetragonal, and orthorhombic, depending on the preparation method and the number of vacancies.[106] $TiO_6$ octahedra form the perovskite-type skeleton, with $La^{3+}$, $Li^+$ and vacancies randomly ordered or with disordered distribution at

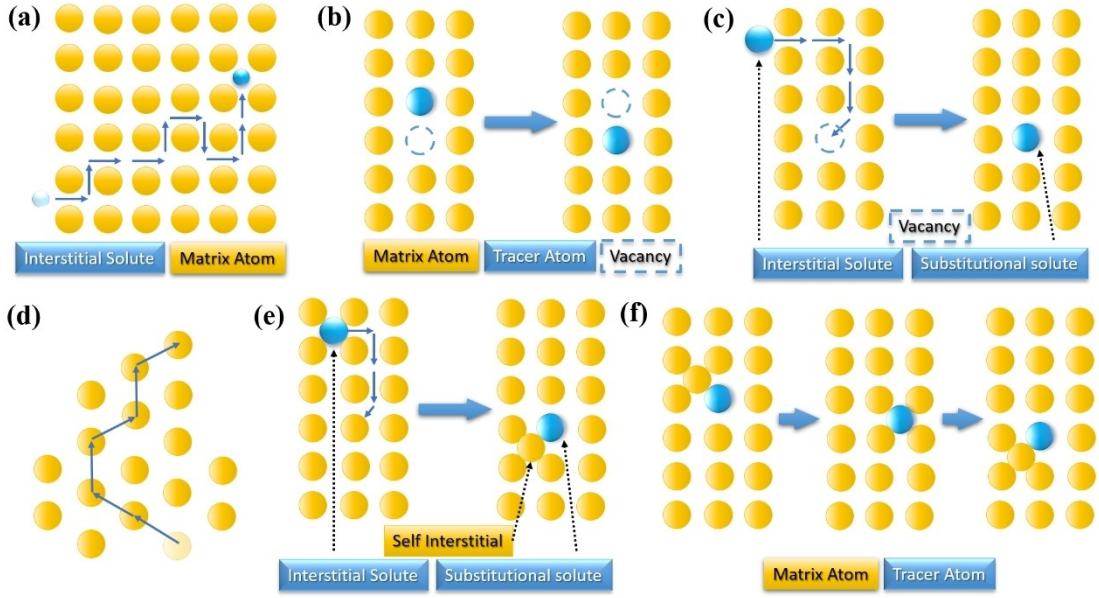


**Figure 3.** Ions transport mechanism: a) Direct interstitial mechanism; b) vacancy mechanism; c) dissociative mechanism; d) collective mechanism; e) knock-off mechanism, and f) interstitialcy mechanism.[105] Adapted from Ref. [105].

A sites. Catti studied the pathway of lithium ions in orthorhombic LLTO using Ab Initio Simulations.[107] As shown in Figure4a and b, two logical models were designed, blue and white spheres, and small gray circles denote La, O, and Li atoms, respectively. Model 1 is more populated than model 2 because it is more favorable in terms of energy. Lithium ions diffuse along with the 2D or 1D pathway in the lithium-containing (001) layer. Model 1 presents a route with alternate "straight" and "90° turn" steps to pass the vacancies on A-sites. In model 2 lithium ions go in a straight line. Since these two models are both in LLTO, the two transportation mechanisms should exist simultaneously.

LATP and LAGP have similar pathways and processes for lithium-ion transportation due to their similar structure, as presented in Figure 4c and d. Rhombohedral LATP and LAGP crystal (space group *R3c*) is composed of corner-sharing $MO_6$ (M = Al, Ti, or Ge) octahedra and $PO_4$ tetrahedra. $Li^+$ occupies Wyckoff site 6b (Li[1] or M1), which coordinates with $O^{2-}$ to

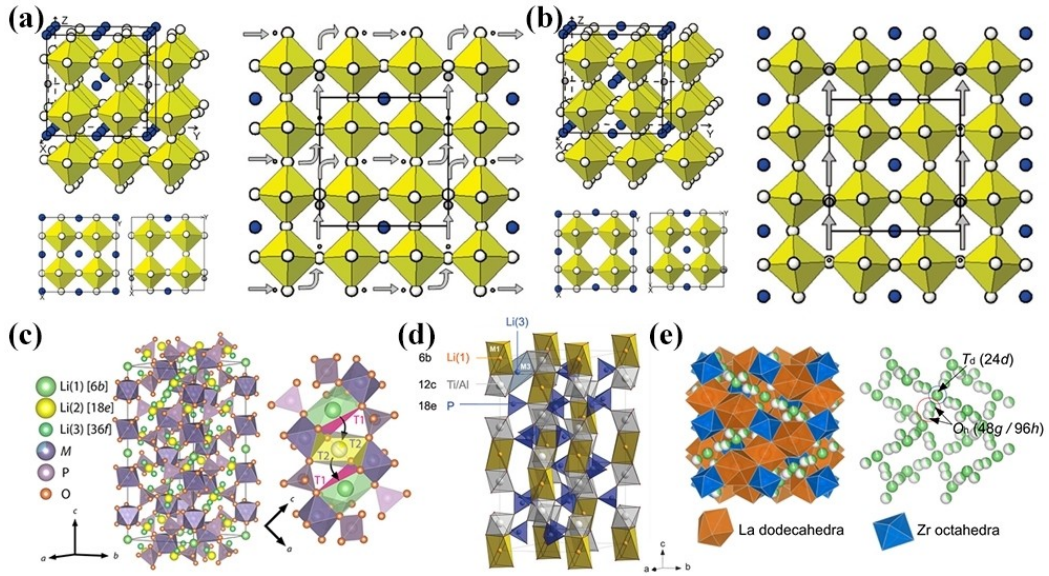


**Figure 4.** a) Model 1 (4La/1La + 1Li + 2□) of $LiLa_5□_2(TiO_3)_8$; b) Model 2 (3La + 1□/2La + 1Li + 1□) of $LiLa_5□_2(TiO_3)_8$[107] (reproduced with permission from Ref. [107], copyright (2008) American Chemical Society). c) Polyhedral representation of the crystal structure of $Li_{1+x}Al_xGe_{2-x}(PO_4)_3$ (M = Al/Ge) and visualization of the hopping path of $Li^+$ through the two triangle areas T1 and T2[108] (reproduced with permission from Ref. [108], copyright (2018) American Chemical Society). d) Crystal structure of LATP-based electrolytes[109] (reproduced with permission from Ref. [109], copyright (2015) The Authors). e) Crystal structure of garnet-type cubic LLZO (SG *Ia3d*)[110] (reproduced with permission from Ref. [110], copyright (2019) American Chemical Society).

form the trigonal antiprismatic unit. $P^{5+}$ occupies Wyckoff site 18e, and $M^{4+}/Al^{3+}$ occupies the 12c position. As the substitution of tetravalent ions by trivalent ions creates an unbalanced charge, the extra lithium ions are introduced into the 18e (Li[2] or M2) and 36f positions (Li[3] or M3).[108,109, 111] The increased lithium-ion concentration can enhance the lithium-ion conductivity. During transportation, lithium ions diffuse from Li(1) across a Li(2) position or two Li(3) positions to another Li(1) position.[108]

As mentioned above, LLZO is a garnet-type material, in which the typical structure is $A_3B_2(XO_4)_3$. A-sites, B-sites, and X-sites are 8-coordinated, 6-coordinated, and 4-coordinated, respectively. There are two types of LLZO: tetragonal LLZO and cubic LLZO. The crystal structure of garnet-type cubic LLZO is presented in Figure 4e, where Li-ions are displayed as partially filled spheres, indicating partial occupancy. For cubic $Li_7La_3Zr_2O_{12}$, high $Li^+$ concentration due to the high occupancy rate of 88% at 48 g/96 h sites leads to high lithium-ion conductivity. $LaO_8$ dodecahedra (La occupies 24c sites) and $ZrO_6$ octahedral (Zr occupies 16a sites) form the framework with the Li sub-lattice. Except for lithium ions occupying 48 g/96 h sites, partial lithium ions also occupy the 24d sites and coordinate with oxygen to form the tetrahedra. Then, $Li_2O_6$ octahedra at 48 g/96 h sites connect with tetrahedra in a coplanar way to form the network for the diffusion of lithium ions.[110,112]

### *1.2.2. Applications and Challenges*

Compared to polymeric electrolytes, ceramic electrolytes have been closer to commercial applications currently. However, several crucial issues remain obstacles to their practical application. Although the lithium-ion conductivity of the ceramic electrolyte can reach $10^{-3}$ S cm$^{-1}$ and the interfacial impedance between the particles in the ceramic sheet can be minimized, the interface contact and interface compatibility of the ceramic polymer and the electrode are challenging. It is well known that achieving intimate solid-to-solid contact is extremely vital but also extremely difficult. Poor solid-to-solid contact commonly results in high interface resistance and the formation of lithium dendrites. In addition, it is almost impossible for ceramic sheets to be defect-free, which also results in the formation of lithium dendrites. Therefore, resolving interface issues is critical for the performance of ceramic electrolytes.

## 1.3. Interface Engineering: Strategy for Solid-State Electrolyte Development

Interface engineering is undoubtedly one of the best strategies to improve the performance of batteries, focusing on physical contact and chemical contact (Figure 5). For physical contact, introducing an alloy layer between the electrolyte and lithium metal or depositing the electrolyte material and the cathode material together are effective and commonly used methods.[113,114] The combination of ceramic electrolyte and polymer electrolyte is also a method to improve the interface contact.[115] Polymers are more liquid-like than ceramics. In order to achieve the same degree of intimate contact, solid-liquid contact has inherent advantages over solid-solid contact in terms of cost and difficulty. However, there are also issues that need to be considered when combining ceramic electrolytes with polymer electrolytes. In the case of the polymer as the substrate, the lithium-ion conductivity of the monolithic electrolyte depends on the ionic conductivity of the polymer. In the case of ceramic material as the principal component, it is necessary to consider whether the interface contact is effectively improved. Therefore, it is important to find the

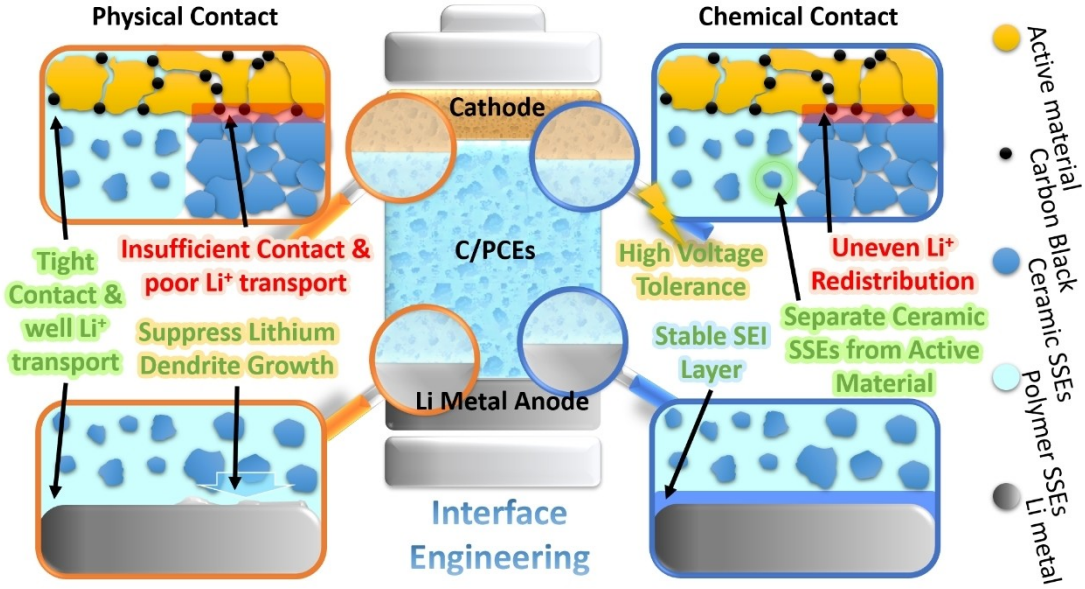


**Figure 5.** Schematic summary of the interface engineering strategies for solid-state electrolyte development.

balance point between the ratio of ceramic electrolyte to polymer electrolyte. Unlike adding a soft layer between the SSEs and the anode, the composite ceramic electrolyte and polymer electrolyte can improve interface contact and enhance various properties of the electrolyte depending on the morphology of the ceramic electrolyte. Besides, the interface layer between the two types of electrolytes is generally modified and facilitates lithium-ion transport.

In addition to reducing interfacial resistance, another effect of improving interface contact is to reduce the formation of lithium dendrites.[116] Tight and uniform interface contact can greatly alleviate the formation of a concentrated local electric field, which is regarded as an important inducement for the growth of lithium dendrites.[117] Adding ceramic electrolyte to polymer electrolyte can prevent the growth of lithium dendrites from two aspects. One is the improvement of the interface contact mentioned above, and another one is that ceramic electrolyte can reduce the current density at the interface area between the electrolyte and the electrodes.[118] It will be discussed in detail in the following sections.

Not only improving physical contact but also improving chemical contact is a crucial goal of interface engineering. Most solid electrolytes have problems with chemical stability, such as the aforementioned sulfide electrolytes. The situation at the interface between the electrolyte and the lithium metal anode is relatively simple. The key problem is that whether the electrolyte can continuously react with the lithium metal. Therefore, the method of introducing a buff layer that is not reactive with lithium metal or can generate a stable SEI layer is usually used to solve this problem.[119–121] The chemical reaction at the interface between electrolytes and cathode is complicated. Even the contact between two different ceramic lithium-ion conductors can lead to resistance.[122,123] Although C/PCEs can block the contact between the ceramic modifier and the active material of cathode, the poor thermal stability, and low oxidation potential of the polymer still limit the improvement effect of C/PCEs on the positive electrode interface. Therefore, C/PCEs with high voltage tolerance are highly expected. Ceramic SSEs such as LLZO and lithium phosphorus oxynitride (LiPON) have voltage windows exceeding 5 V, while the decomposition voltage of the most commonly used polymer electrolyte PEO is lower than 3.8 V. Therefore, compositing ceramic SSEs with polymer SSEs usually increase the decomposition voltage of the polymer. Better than PEO, the decomposition voltage of the PAN system is generally between 4.3- 5.0 V (vs. $Li/Li^+$), and the electrochemical window of PMMA series gel polymer electrolyte is generally above 4.6 V (vs. $Li/Li^+$). Therefore, using PAN, PMMA, PVDF, and other polymers with higher decomposition voltage to combine with ceramic materials can get a better effect.[124] Zhang et al. prepared the C/PCEs of LLZTO/PVDF/LiTFSI, which can enlarge the electrochemical window to 4.8 V.[125] Zhu et al. adding the MIL-53(Al) as the modifier into the PEO electrolyte, the obtained C/PCEs can work at a high potential of 5.10 V at 120 °C.[126] Hu et al. synthesize the C/PCEs with thiol-modified silica nanoparticles and poly(ethylene glycol) diacrylate via thiol-acrylate photopolymerization under UV irradiation. The measured electrochemical window reaches 5 V.[127] It is of great significance to study high-voltage-tolerated composite electrolytes. Due to the expansion of the electrochemical window, the energy density of the battery can be increased by 20–50%.[128] Therefore, C/PSEs could be a general solution because it can achieve excellent improvement effects on both the physical contact and chemical contact issues that are concerned by interface engineering.

## 2. Ceramic/Polymer Composite Solid-State Electrolyte

It is a logical and sensible choice to combine polymer electrolytes with ceramic electrolytes. Poor contact with the electrode is an unavoidable disadvantage of ceramic electrolytes. Because it is difficult to keep the electrode and electrolyte in close contact, in many cases, the interface needs to be wetted by adding a little ionic liquid or liquid electrolyte.[129] This enables the delivery of the intrinsic high ionic conductivity of the ceramic electrolyte. For polymer electrolytes, the ionic conductivity is greatly affected by temperature resulting in poor ionic conductivity at room temperature. The addition of a ceramic modifier can greatly improve the ionic conductivity of polymer electrolyte, which makes it possible to use at room temperature. We believe that the mechanism of the C/PCEs performance improvement and the lithium-ion transport mode is influenced by the structure of the C/PCEs more so than the type of ceramic modifiers. Therefore, we regard the polymer electrolytes as the matrix and classify them according to the morphology of the ceramic modifiers added. Lithium-ion conduction may vary depending on whether the modifier is active or inert, but the structural effect is still the dominant component.

An overview of C/PCEs with ceramic modifier from 0D to 3D structure is provided below. The summary mainly involves the improvement of ionic conductivity, the enhancement of electrochemical stability, the enhancement of polymer mechanical strength, the flexibility of adjusting properties for various demands, the resistance to lithium dendrites, and preparation difficulty. The results are visually presented in the radar maps in Figure 6.

The ability to resist lithium dendrites can be significantly improved by 0D C/PCEs with the simplest preparation method. Moreover, the amount and location of 0D modifiers are flexible. These advantages and the mechanism of lithium-ion transport in 0D C/PCEs will be the focus of later discussion. Ionic conductivity is markedly improved in 1D C/PCEs, due to the continuous lithium-ion transport pathway and a large number of vacancies provided by 1D modifiers. Compared with 0D and 1D C/PCEs, 2D C/PCEs are relatively mediocre. The preparation methods of 3D C/PCEs are varied and novel. The monolithic network constructed can provide a continuous pathway like 1D C/PCEs, and also has excellent resistance to lithium dendrites like 0D C/PCEs.

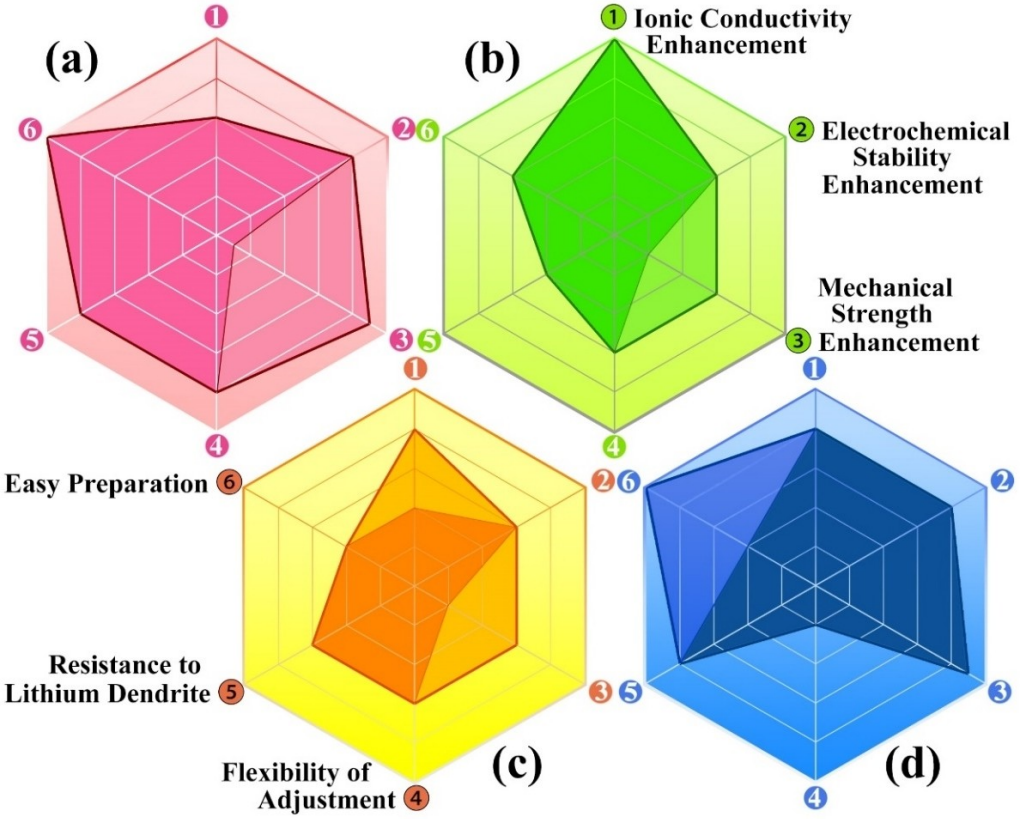


**Figure 6.** Overview of a) 0D, b) 1D, c) 2D, and d) 3D composite ceramic polymer electrolyte in terms of six aspects (ionic conductivity enhancement, electrochemical stability enhancement, mechanical strength enhancement, flexibility, resistance to lithium dendrite formation and preparation simplicity). Darker shaded areas represent fixed values, light areas represent values that can change.

### 2.1. Zero-Dimensional Ceramic Materials/Polymer Composite

Zero-dimensional composites have the simplest preparation technologies of all the composites. In general, the 0D structure usually refers to ceramic materials added into the polymer in the form of powder or nanospheres. In recent years, more work has been done on active modifiers than on inert modifiers, among which garnet-type materials are the most widely used. The polymer matrix used for most of these 0D composites is usually PEO.

There are two phases in polymer electrolyte, i.e., crystalline phase and amorphous phase. The transport of lithium ions in the polymer depends largely on the free movement of the chains in the amorphous phase. Therefore, as illustrated in Figure 7, the main purpose of introducing ceramic modifiers, whether active or inert, is to reduce the crystallinity of the

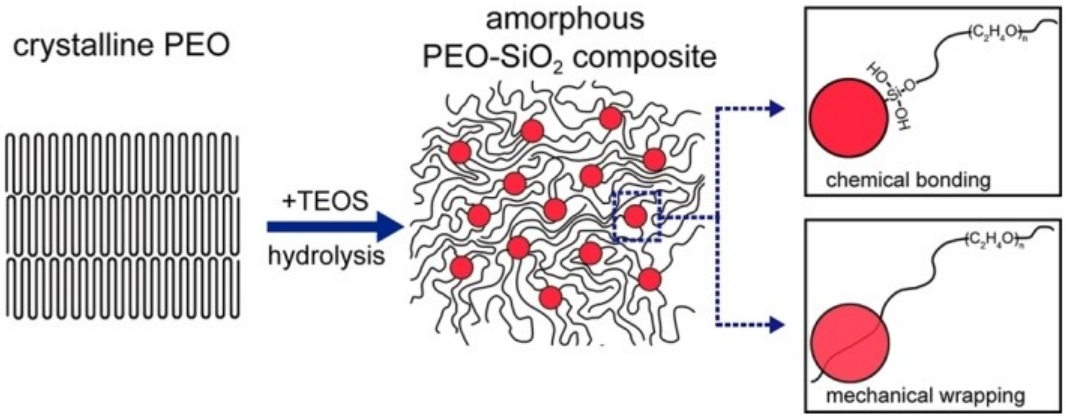


**Figure 7.** Schematic diagram of the reduction of crystallinity of PEO using chemical bonding and mechanism wrapping mechanisms.[134] Reproduced with permission from Ref. [134]. Copyright (2015) American Chemical Society.

polymer.[21,76, 130–139] For instance, in the work of Zhao et al., after adding LGPS ($Li_{10}GeP_2S_{12}$) powders into the PEO-based electrolyte, the glass transition temperature ($T_g$) reduced to −41.6 ~ −41.3 °C from −39.6 °C. The melting temperature ($T_{m2}$) dropped from 66.5 °C to 57.8 ~ 59.9 °C. Generally, the decrease in $T_g$ and $T_{m2}$ means an increase in the amorphous phase and a decrease in the crystalline phase. As a result, the $PEO_{18}$-LiTFSI-1 % LGPS sample delivered a lithium-ion conductivity of $1.18\times10^{-5}$ S cm$^{-1}$ at 25 °C and $1.21\times10^{-3}$ S cm$^{-1}$ at 80 °C while that of a PEO-only membrane was $6.16\times10^{-6}$ S cm$^{-1}$ at 25 °C and $7.98\times10^{-4}$ S cm$^{-1}$ at 80 °C. However, the authors pointed out that adding ceramic powders had two opposite effects. On the one hand, the uniform distribution of ceramic powders helps to prevent polymer crystallization and create a large number of interface regions, so it has an advantage over nanoscale powders with a larger specific surface area than micron-sized powders. On the other hand, the particles of the powder can act as cross-linking sites for the polymer, creating new lithium-ion transport pathways independent of the movement of the chain segment, so too much powder can lead to increased crystallinity.[139]

The use of some atypical modifiers can also reduce the crystallinity of the polymer through unique mechanisms. Yang et al. added g-$C_3N_4$ into the PEO-based electrolyte to obtain C/PCEs with low $T_{m2}$ of 48.7 °C (10 wt.% g-$C_3N_4$). The g-$C_3N_4$ is prepared from urea by thermal polymerization. After preparation, the residual -$NH_2$ or -NH groups in g-$C_3N_4$ can form a hydrogen-bond with the oxygen atom in PEO, which can inhibit the folding of the PEO chain segment and prevent the crystallization of PEO.[138] Though all-ceramic modifiers can reduce the crystallinity of polymer, it is difficult for inert modifiers to achieve as high ionic conductivity as active modifiers, especially when ceramic phase content is high. For example, 70 wt.% LAGP in PEO can produce a higher ionic conductivity of $1.0\times10^{-5}$ S cm$^{-1}$ than that of 70 wt.% $Al_2O_3$ in PEO ($7.2\times10^{-7}$ S cm$^{-1}$).[132] However, even active modifiers may have poor contact with the polymer and lead to a decrease in lithium-ion conductivity. Huang et al. attributed this to the high surface energy of the nanoparticles. Therefore, they prepared a dopamine-modified LLZTO nanoparticle, which ensures close contact between LLZTO and PEO, so that the LLZTO nanoparticle powders can be evenly dispersed in PEO. The ionic conductivity of the dopamine coated LLZTO/PEO sample ($1.15\times10^{-4}$ S cm$^{-1}$) is double that of the sample without dopamine coated.[131] In addition, the added ceramic powder can usually be regarded as a Lewis base, so the Lewis acid-base interaction between lithium salt and ceramic powder surface can promote the dissociation of lithium salt, produce more free carriers, and enhance the ionic conductivity. At the same time, it can also reduce the complexation effect of polymer on lithium ions, making lithium ions easier to transfer, thus increasing the transference number of lithium ions. This mechanism generally exists in various systems, such as LLZO-PVDF-LiTFSI,[140] LLZTO-PPC-LiTFSI,[141] $TiO_2$-PEO-$LiClO_4$,[142] LLZO-PVDF-$LiClO_4$.[143,144]

Another great benefit of the addition of ceramic modifiers is the improvement of electrolyte stability and the ability to prevent Li dendrite growth,[145] which are manifested in the increase of polymer decomposition voltage[146,147] and the decrease of current density at the electrolyte/anode interface. Almost all studies mention improvements in these aspects, although some did not suggest that the addition of ceramic modifiers was beneficial for the reduction of polymer crystallinity and the improvement of lithium-ion conductivity .[148] As shown in Figure 8a and b, linear sweep voltammograms (LSV) can reveal the decomposed voltage of the electrolyte membrane. Under a sweep rate of 1 mV s$^{-1}$, a 50 wt.% LLZO added PVDF-HFP hybrid membrane decomposed at a higher voltage of ~ 5.3 V (vs. $Li^+$/Li) than that of pure PVDF-HFP film, which is about 4.5 V (vs. $Li^+$/Li).[149] Even greater improvements have been made in the PEO-based electrolyte system. The upper limit of the electrochemical window was raised from 3.8 V to 5.2 V (vs. $Li^+$/Li) due to the addition of 10 wt.% $LiAlO_2$ and 15 % succinonitrile.[150] Furthermore, the decomposition potential of LAGP added PEO electrolyte could increase to 5.12 V (vs. $Li^+$/Li). As LAGP and PEO are both polar molecules, the dipole-dipole interaction between them changes the electron transition energy level of PEO, thus increasing the oxidation decomposition potential of PEO.[151]

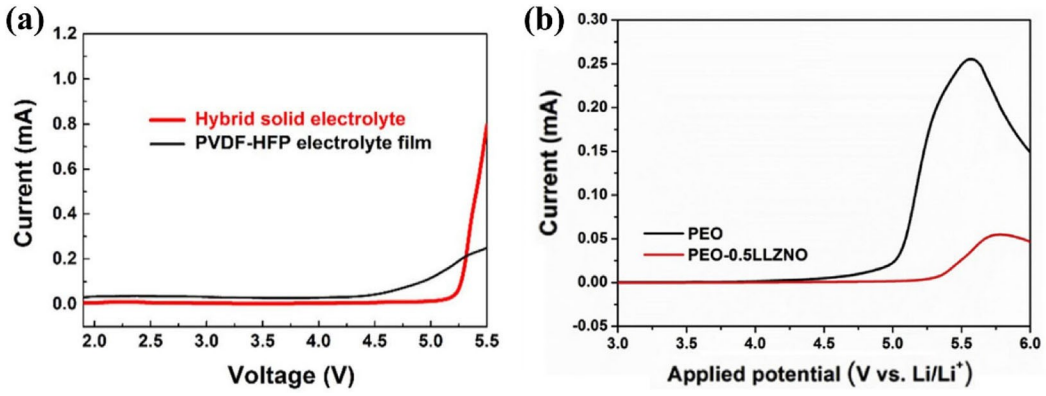


**Figure 8.** a) Comparison of liner sweep voltammograms of pure PVDF-HFP electrolyte and the HSE.[149] Reproduced with permission from Ref. [149]. Copyright (2018) Elsevier; b) LSV pure PEO and PEO-0.5LLZNO.[146] Reproduced with permission from Ref. [146]. Copyright (2019) Elsevier.

Lithium dendrites can easily penetrate the ceramic electrolyte or polymer electrolyte membrane, but the structure of C/PCEs is effective in inhibiting the growth of lithium dendrites. One reason is that the addition of ceramic modifiers improves the overall mechanical strength of the electrolyte.[131] Another more important reason is that the uniform distribution of ceramic modifiers in the polymer makes the distribution of lithium ions more uniform (Figure 9 a-d).[152–154] When the lithium disassociates, a large number of free lithium ions and the corresponding anions filled the electrolyte. Under the applied external electric field, the anion will move in the opposite direction to that of lithium ions, which will hinder the migration of lithium ions. Meanwhile, due to the difference in electric field intensity in a different part of the electrolyte, lithium ions will form a concentration gradient, which will gradually increase with time. This is not conducive to uniform deposition of lithium ions, which leads to the formation of lithium dendrites. In return, lithium dendrites will further aggravate the heterogeneous distribution of lithium ions, forming a positive feedback cycle. With the uniform distribution of ceramic powders, lithium ions can be fixed and weaken the concentration gradient of lithium ions, thereby providing a more suitable environment for uniform deposition of lithium ions.[154]

The function of adjusting current density by nanoparticles may require a dynamic process. According to the voltage profiles during the stripping/plating experiment at 70 °C with a current density of 0.1 mA cm$^{-2}$ in the work of Zagórski et al. (Figure 9e), the response voltage of 10 vol% LLZO added electrolyte was unstable and much more polarized than that of pure PEO electrolyte during the first 70 hours of the reversible Li plating/stripping cycles. The authors think that this is caused by the direct contact of LLZO particles in the hybrid electrolyte with lithium metal because PEO cannot completely cover all-ceramic particles or electrodeposited lithium can reach the LLZO particles near the Li anode. There, a hypothesis was proposed, as illustrated in Figure 9f–i. Figure 9f and h show the initial stages of pure polymer electrolyte and C/PCEs, respectively. The process of electrochemical deposition and stripping may produce direct contact and free volume between lithium and LLZO particles, respectively. After several cycles, electrolyte tended to form a state that completely isolated LLZO particles and the lithium metal anode by an extremely thin layer of PEO. In this state, the lithium ions can realize uniform deposition. Moreover, the authors also highlighted that there is lithium ion exchange between the LLZO phase and the PEO phase, which can minimize the concentration gradients near the interface between electrolyte and anode, leading to homogeneous electrodeposition.[155] Wang et al., through the addition of a 100 nm PEO modification layer between the hybrid electrolyte and the lithium electrode that was originally intended to improve contact, also facilitated the reduction of lithium ion concentration gradients and uniform deposition.[151]

### 2.2. One-Dimensional Ceramics Materials/Polymer Composite

One-dimensional ceramic modifiers refer to nanorods or nanofibers of various materials, which can produce different effects to those of 0D nanoparticles due to their extension in a certain

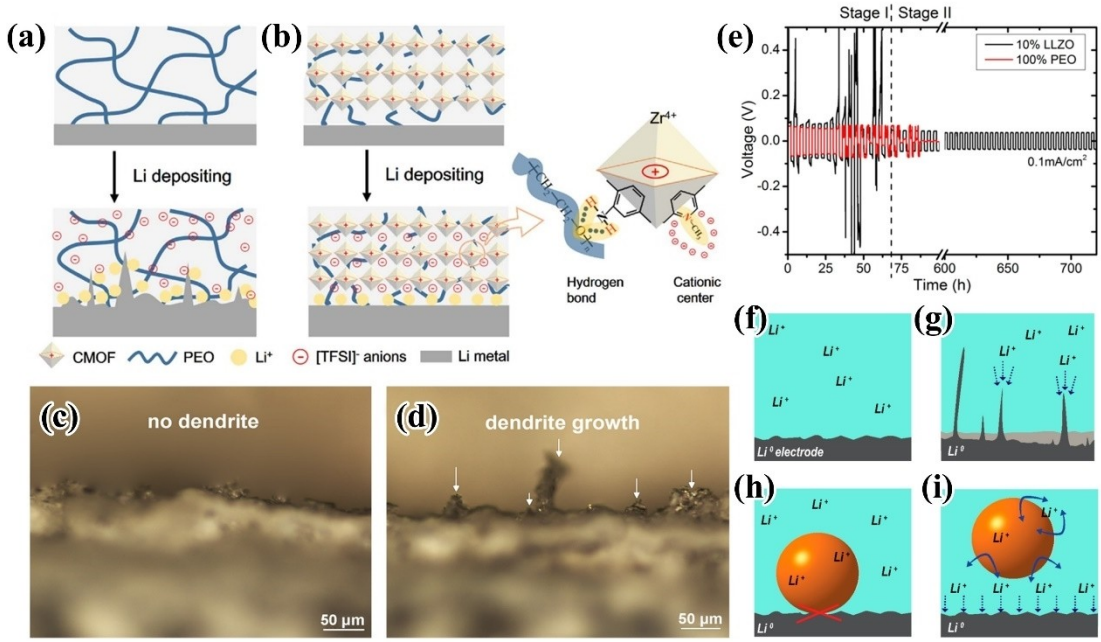


**Figure 9.** a, b) Schematic of the Li deposition behavior with (a) PEO(LiTFSI) electrolyte and (b) anion-immobilized P@ cationic-MOF electrolyte[152] (reproduced with permission from Ref. [152], copyright (2019) Elsevier). c) Li/PEO:LLZTO/Li after cycling over 700 h (no dendrites) and d) Li/PEO: LiTFSI:LLZTO/Li after cycling for about 25 h (large dendrites)[153] (Reproduced with permission from Ref. [153], copyright (2016) Elsevier). e) Voltage profiles of the symmetric Li metal cell with pure PEO(LiTFSI) and C/PCEs; proposed model of local Li+ transport at various stages of Li electrodeposition in (f, g) PEO(LiTFSI) reference electrolyte and (h, i) LLZO – PEO(LiTFSI) C/PCEs[155] (reproduced with permission from Ref. [155], copyright (2019) American Chemical Society).

direction. Electrospinning is the most common and effective method to obtain nanofibers. The nanofibers produced by electrospinning are normally randomly interlaced to form a 3D frame structure. However, for LIBs, lithium ions migrate in the vertical direction to the surface of the electrode under the external electric field. Therefore, the nanofibers parallel to the surface of the electrode do not play a great role in lithium-ion transport, but rather as the cross point and in supporting the whole structure (Figure 10).[156,157] As a consequence, even though the fiber constitutes a 3D network structure, we still consider it as a 1D ceramic modifier.

As previously discussed, there are four main purposes or effects produced by uniformly distributing nanoparticles into polymer electrolyte: reducing the polymer crystallinity, increasing the concentration and mobility of lithium-ion Lewis acid-base reactions, improving the thermal and electrochemical stability of polymers and preventing lithium dendrites. When using nanofibers or nanorods, the first three functions have been examined in several studies, while the prevention of lithium dendrites is rarely discussed. This is probably because nanofibers and nanorods are less evenly dispersed than nanoparticles, thus cannot effectively reduce the concentration gradient.

The biggest advantage that nanofibers or nanorods have over nanoparticles is their ability to provide a continuous, long-distance lithium-ion transport pathway.[156,158–162] In the work of Hua et al., a 3% $TiO_2$ filled PPC electrolyte presented the best ionic conductivity of $1.52\times10^{-4}$ S cm$^{-1}$ at room temperature and a capacity of 162 mAh g$^{-1}$ with a high capacity retention of 93%. The 3% $TiO_2$ nanorods cannot form an overall lithium-ion transport network in the electrolyte, but lithium-ion transport can be improved in some areas (Figure 11a).[159] Zhai et al. prepared a vertically aligned LATP modifier by using an ice-templating-based method, as displayed in Figure 11b and c. The PEO/PEG electrolyte with this type of LATP modifier exhibited an ionic conductivity of $5.2\times10^{-5}$ S cm$^{-1}$ at room temperature, while that of PEO/PEG electrolyte with LATP nanoparticles and pure PEO/PEG electrolyte were $1.5\times10^{-5}$ S cm$^{-1}$ and $7.7\times10^{-6}$ S cm$^{-1}$ respectively. In the ceramic fiber/polymer composite electrolyte prepared by the ice-templating-based method, the content of LATP is about 40%. Such a large number of nanowires can form a highly efficient percolation network, providing a continuous conduction path for lithium-ion transmission over longer distances.[156]

### 2.3. Two-Dimensional Ceramics Materials/Polymer Composite

Unlike nanoparticles or nanofibers, 2D nanosheets are rarely used as ceramic modifiers. One of the reasons is that it is difficult for nanosheets to form continuous paths like nanowires. The other is that when the size of the nanosheets is large, the nanosheets parallel to the electrode surface will result in a longer and more convoluted lithium-ion transmission pathway. In addition, the polymer crystallinity cannot be efficiently reduced if the nanosheets are too large. Therefore, many studies have tried to synthesize smaller size nanosheets.[163] Not only can reducing the size of nanosheets effectively avoid the above disadvantages, but smaller nanosheets can provide a larger effective interface than nanoparticles. Creating a way for lithium ions to penetrate the sheets is another way to solve this problem. Sun et al. synthesized g-$C_3N_4$ nanosheets by thermal oxidation etching. As shown in Figure 12a, g-$C_3N_4$ has a planar structure rich in nitrogen atoms, which can interact with the lithium salt and increase the concentration of lithium ions. More importantly,

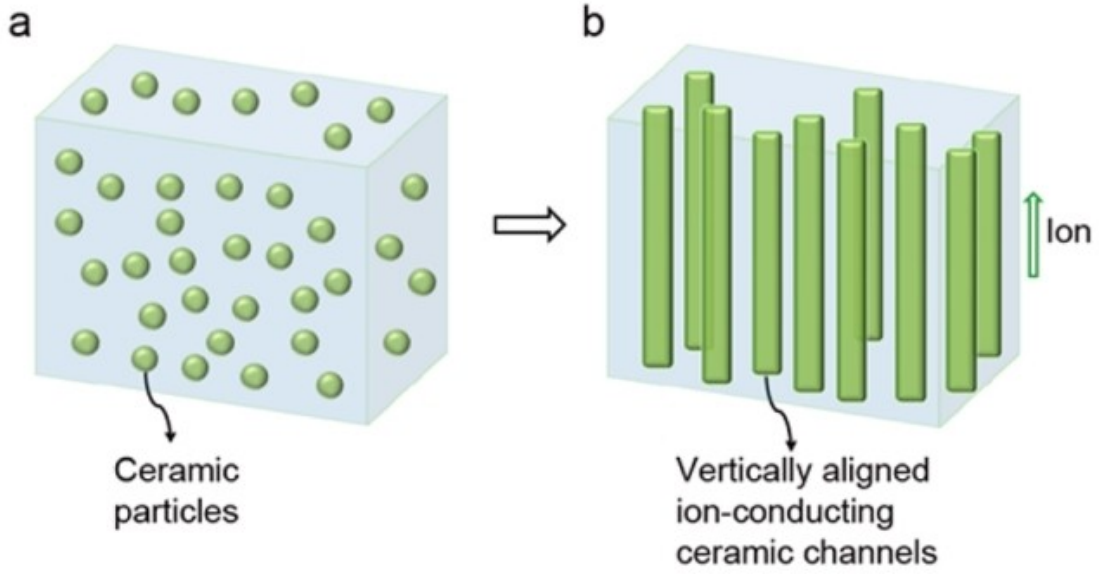


**Figure 10.** Schematic of vertically aligned and connected ceramic channels for enhancing ionic conduction. a) Ceramic particles are randomly dispersed in the polymer matrix, where ion transport is blocked by the polymer matrix with a low conductivity. b) Vertically aligned and connected structure to facilitate ion transport, which can be realized by the ice-templating method.[156] Reproduced with permission from Ref. [156]. Copyright (2017) American Chemical Society.

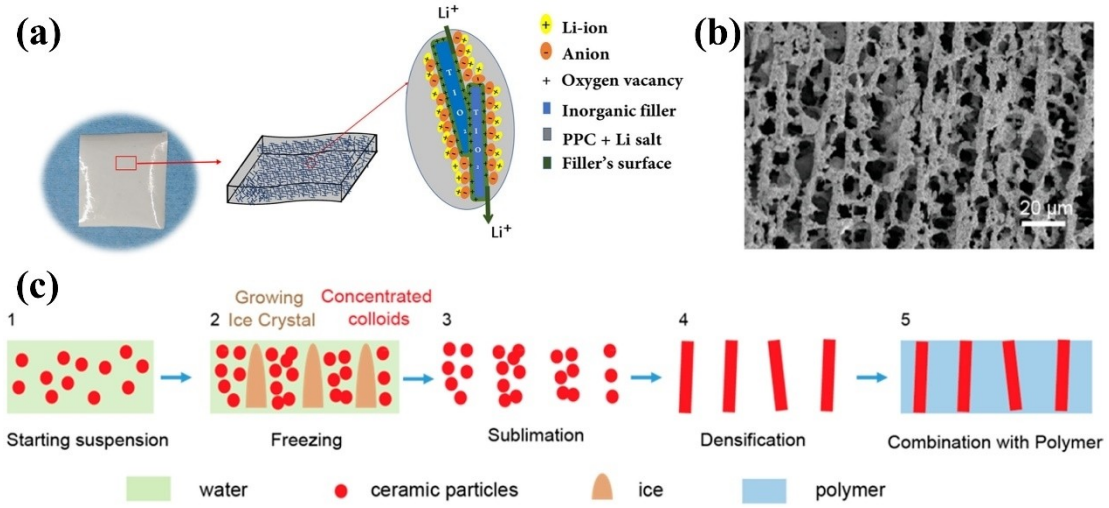


**Figure 11.** a) Schematic image of lithium-ion transport in $TiO_2$ nanorod-filled C/PCEs[159] (reproduced with permission from Ref. [159], copyright (2019) Wiley-VCH); b) fabricated C/PCEs by ice-templating-based method and c) ice-templating process[156] (reproduced with permission from Ref. [156], copyright (2017) American Chemical Society).

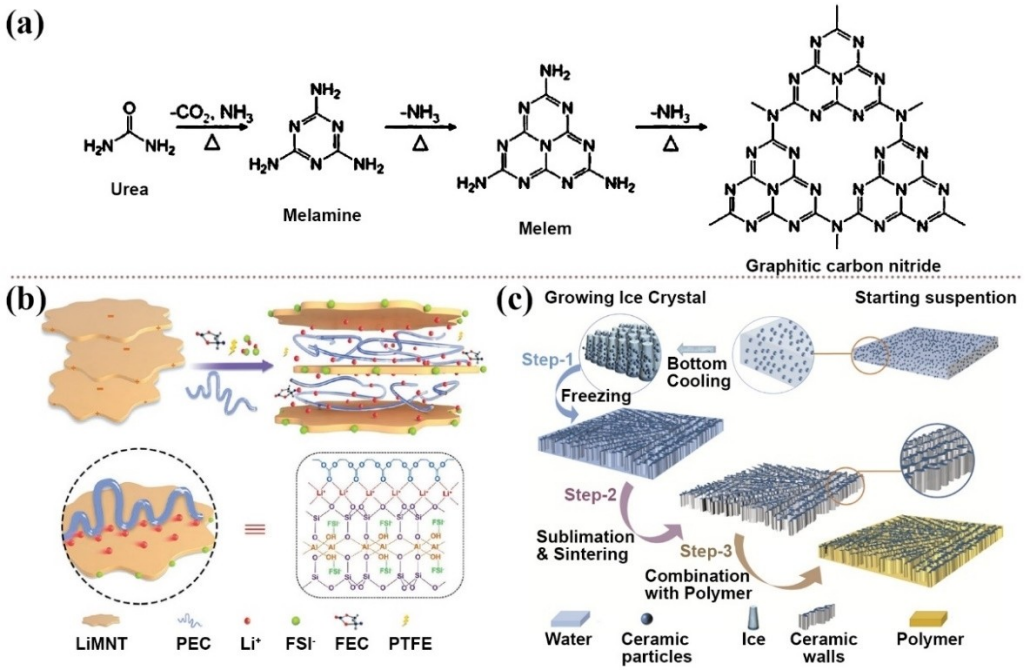


**Figure 12.** a) Reaction pathway for the self-polymerization of urea into g-$C_3N_4$ nanosheets at high temperature in air,[164] (reproduced with permission from Ref. [163], copyright (2019) Royal Society of Chemistry). b) Mechanism of enhanced ion transference number for intercalated PEC-LiMNT CSE[165] (reproduced with permission from Ref. [165], copyright (2019) Wiley-VCH). c) The schematic of preparation process of the ice-templated LAGP/PEO composite electrolyte[166] (reproduced with permission from Ref. [105], Copyright (2019) Elsevier).

the widely distributed defects allow lithium ions transport across the nanosheet vertically, which is a unique property different to other nanosheets.[164]

Given the large effective area of nanosheets, high ionic conductivity can also be obtained. As shown in Figure 12b, PEC was inserted into the interlayer between lithium montmorillonite (LiMNT) sheets. There are various groups on the different surfaces of LiMNT: -Si-O–Si- groups on upper and lower surfaces and -Al-OH groups on the edge-shared surface. This results in upper and lower surfaces having negative charges and the edge-shared surface having positive charges. The lithium salt anions tend to locate on the edge-shared surface, while lithium ions prefer to concentrate in the interlayer region. With the complicated electrostatic interactions in the intercalation area, there is orderly lithium-ion transport, which shortens the transmission path.[165]

While nanosheets may create a longer lithium ions transport pathway, 2D ceramic modifiers perpendicular to the

surface of the electrode alleviate this concern. The ceramic walls of LAGP can be obtained by the process displayed in Figure 12c. With 40 vol% content of LAGP, the C/PCEs can deliver a high ionic conductivity of $1.67\times10^{-4}$ S cm$^{-1}$ at room temperature, which is 6.2 times higher than random distribution LAGP/PEO electrolyte. Moreover, even compared with well-aligned ceramic nanowires, the LAGP walls/PEO is still 2.8 times higher.[166]

### 2.4. Three-Dimensional Ceramics Materials/Polymer Composite

Unlike nanoparticles, nanowires, and nanosheets, there are many kinds of 3D ceramic structures. Although most of them are network structures, the 3D structures discussed in this section are prepared as a whole, which is different from the network structures constructed by nanofibers.[167] As shown in Figure 13a, Bae et al. synthesized an LLTO network by dissolving the LLTO precursor in a hydrogel-crosslinked network that is eventually removed. The high ionic conductivity of $8.8\times10^{-5}$ S cm$^{-1}$ at room temperature can be attributed to the continuous interface pathway and abundant surface vacancies for lithium ions to hop on LLTO.[168] In contrast, a Ga-doping LLZO 3D network was fabricated by covering the sacrificial polymer template with Ga-doping LLZO slurry. This method is called the polymeric sponge method (Figure 13b–d).[169] It is even simpler to prepare 3D microporous LLZO frameworks using absorbent cotton as the template with ionic conductivity of $8.9\times10^{-5}$ S cm$^{-1}$ at room temperature.[170] However, the monolithic 3D networks prepared by various methods are not better than the 3D network constructed by 1D nanofibers.[78,162] That may be because in the C/PCEs with 3D ceramic network prepared using a template as the modifier, the ceramic modifier content is high and fixed, and cannot be adjusted to the most appropriate content. From this perspective, the addition of 1D nanofibers may not be as simple, but it is more flexible.

Some morphologies are not a 3D network structure, such as core-shell spheres and hollow spheres. They can also be regarded as 0D ceramic modifiers. Since the hollow spheres have outer and inner surfaces for modifying, which are unlike nanoparticles, these spheres are classified as 3D materials here. In these situations, these specially designed morphologies have some specific functions. For instance, compositing PEO with $SiO_2$ spheres coated with boron-included polymers can improve the thermal/dimensional stability of PEO and promote the dissolution of lithium salts[171] while the $SiO_2$ hollow spheres can significantly prevent lithium dendrites (Figure 14a).[172] Zhang et al., demonstrated that $Al_2O_3$ modifiers had a 3D honeycomb structure, but enhanced the ionic conductivity in the same way as vertically aligned nanofibers (Figure 14b and c).[173]

### 2.5. Mechanism of Lithium-Ion Transport in C/PCEs

The mechanism of lithium-ion transport in the hybrid electrolyte with active modifiers is very complex, resulting in a significant debate in the literature. It is well-established that the crystalline phase in the polymer accounts for a large proportion below the $T_g$, while the amorphous phase for Li+ transporting accounts for a large proportion above the $T_g$. As mentioned above, the addition of ceramic materials could reduce the crystallinity and $T_g$ of the polymer. Therefore,

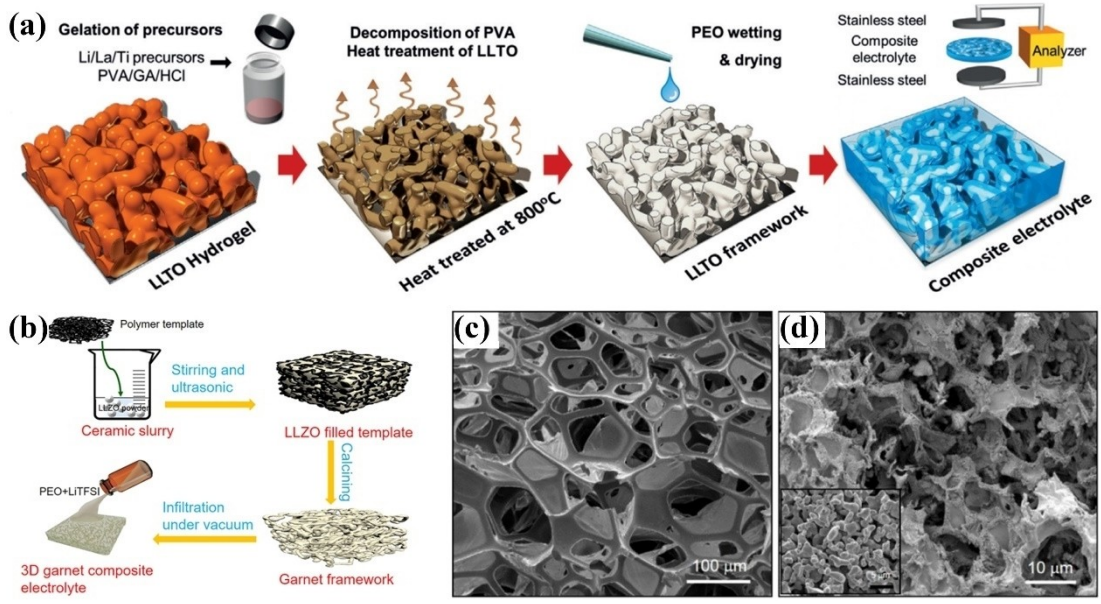


**Figure 13.** a) Schematic representation of the synthesis of LLTO framework C/PCEs: LLTO hydrogel, decomposition and heat treatment, PEO wetting and drying, and electrochemical analysis of C/PCEs[168] (reproduced with permission from Ref. [168], copyright (2018) Wiley-VCH). b) Synthesis procedure of 3D garnet-type C/PCEs, c) SEM image of the polymer template, d) SEM images of the garnet-type framework[169] (reproduced with permission from Ref. [169], copyright (2019) American Chemical Society).

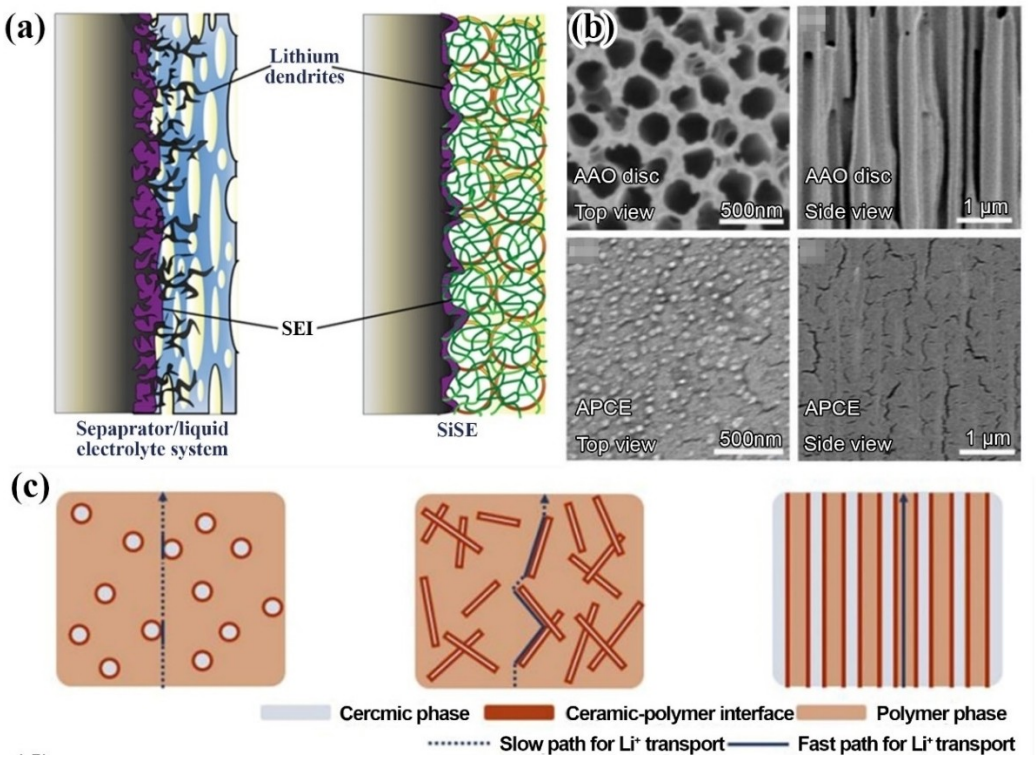


**Figure 14.** a) The suppression mechanism for Li dendrite growth by capitalizing on $SiO_2$ hollow nanosphere-based C/PCEs (SiSE) as SSEs[172] (reproduced with permission from Ref. [172], copyright (2016) Wiley-VCH). b) SEM characterizations of pristine AAO and SPE infiltrated AAO; c) schematics of C/PCEs with three types of geometrical structures of ceramic-polymer interface[173] (reproduced with permission from Ref. [173], copyright (2018) American Chemical Society).

although both the data obtained above or under $T_g$ were used in the article, the conclusions obtained from them are consistent. There are three main opinions on lithium-ion transport in C/PCEs: first, lithium-ion transport in the bulk of polymer and the interface between ceramic particles and polymer matrix; second, lithium-ion transport in the bulk of ceramic phase; third, the addition of ceramic modifiers does not enhance ionic conductivity. Zagórski et al. found that when the added amount of LLZO exceeds 40%, the ionic conductivity drops rapidly and is close to that of the LLZO free PEO electrolyte. The increase of ionic conductivity is mainly due to the decrease of polymer crystallinity and enhanced chain segment movement when ceramic modifiers are not added. This conclusion is further confirmed by replacing LLZO of partial cubic phase with the tetragonal phase and obtaining similar lithium ionic conductivity. This is due to the excessive ceramic modifier limiting the movement of the polymer chain segment, resulting in a decrease in the rate of ion migration.[155] Both Huo et al.[152] and Zhang et al.[153] attribute the enhanced ionic conductivity to the pathway available for high-speed transmission of lithium ions along the area of the interface. This is because there is a small amount of added MOF (12.5 vol%) or LLZTO (12.7 vol%) in their work. In fact, the researchers who hold the first view believe that the transportation of lithium ions in the polymer and interface is dominant when the content of active modifier is relatively small.[154] Take Chen et al.'s study on the content of active modifiers as an example. After exploring the ion conductivities of lithium ions from "ceramic-in-polymer" electrolyte to "polymer-in-ceramic" electrolyte, the critical role of the permeability threshold of LLZO can be observed.[174] The permeability threshold is related to the content of LLZO, when the content is less than the permeability threshold, lithium ions are primarily conducted through the transmission path in the polymer bulk and interface region; when the content is greater than the permeability threshold, the ceramic modifier will participate in the transport of lithium ions. Since the ionic conductivity of the active modifier is generally much higher than that of the polymer matrix, the transport of lithium ions in the ceramic modifier will dominate in this case.

In some studies, the transport path of lithium ions is revealed by tracking the $^6$Li isotope. This method confirms in which phase lithium ions are transferred based on the content change of $^6$Li in different phases before and after cycles. Many studies have found that the content of $^6$Li in the ceramic phase increases greatly after cycles, so it is believed that lithium ions mainly migrate in the ceramic phase, which is the second view.[70,175] Since the C/PCEs used in these studies mostly contain a large number of ceramic modifiers,[151] this conclusion does not actually conflict with the first view. However, as mentioned above, in the work of Zagórski et al., lithium-ion exchange exists between ceramic particles and polymer electrolyte, as represented in Figure 15a. The ion exchange process not only occurs at the surface of the ceramic particles and interfacial region but also in the bulk of ceramic and polymer phases.[155] Therefore, the change of $^6$Li content may

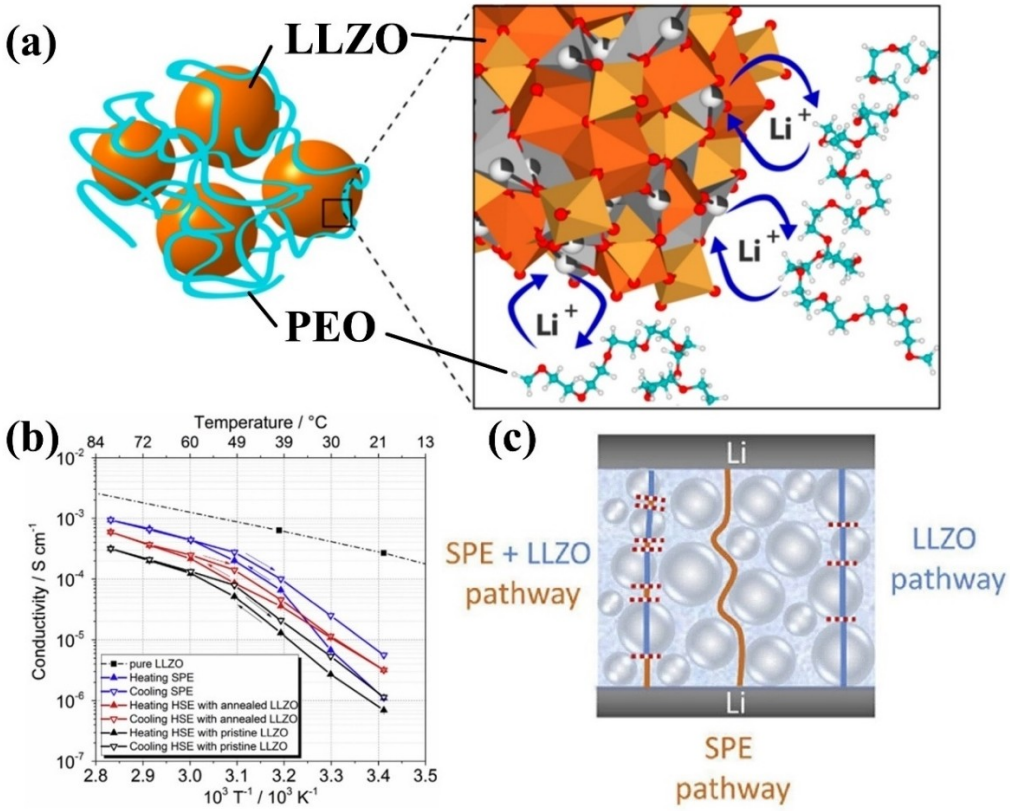


**Figure 15.** a) Schematic illustration of the interfacial Li + exchange between LLZO particles and PEO(LiTFSI) matrix[155] (reproduced with permission from Ref. [155], copyright (2019) American Chemical Society). b) Arrhenius conductivity vs temperature plot of the solid polymer electrolyte and hybrid SSEs (containing pristine and annealed LLZO) samples; c) schematic model of possible lithium-conducting pathways through the hybrid SSEs samples[148] (reproduced with permission from Ref. [148], copyright (2017) Elsevier).

be of limited usefulness in determining the transport mechanism.

The third view is the exact opposite of the previous two. Marlou et al. predicted that since the ionic conductivity of ceramic modifiers is higher than that of polymer electrolytes, the ionic conductivity of hybrid electrolytes would be higher than that of pure polymer electrolytes. However, they found the opposite, as shown in the Figure 15b. The conductivity declines of the hybrid electrolyte compared with the polymer electrolyte is consistent with the volume fraction of LLZO, so LLZO is determined as the inert phase. In this case, the cross-sectional area in the polymer matrix was reduced, and a convoluted longer pathway needs to be passed by lithium ions (Figure 15c).[148] It can be seen that the transport mechanism of lithium ions in the hybrid electrolyte is extremely complex. Therefore, the development of in-situ observation is of great importance to the study of SSEs mechanisms.

There is a new lithium-ion conduction mode for LLTO and LLZO nanowires that nanoparticles do not have. LLTO and LLZO possess many vacancies on their surface. When a continuous pathway was formed by nanowires, lithium ions can achieve rapid long-distance transportation along with the fiber by hopping and replacing the adjacent vacancy.[78,176, 177] Even ceramic materials with few vacancies can be modified to increase the number of vacancies to realize a similar effect. For example, LATP nanoparticles were mixed with PAN to obtain nanofibers by electrospinning, which were directly added to a $PEO_8$-LiTFSI electrolyte to obtain a hybrid electrolyte. Since there are no lithium salts in the PAN, lithium ions in LATP will be absorbed by PAN. Thus, the number of lithium vacancies on the surface of LATP is increased, which improves ionic conductivity.[178]

Another way to increase the migration capacity of lithium ions is to enhance the Lewis acid-base reaction. This can be achieved by modifying the morphology of nanofibers. According to Yu et al., many mesopores are produced in $SiO_2$ nanofibers by $Li_2SO_4$ doping, which can improve the wettability with PEO. This further leads to the facilitation of Lewis acid-base interactions. Liu et al. chose $Y_2O_3$ doped $ZrO_2$ (YSZ) nanowires as the modifier for PAN/$LiClO_4$ electrolyte.[67] There is a high concentration of oxygen vacancies on the surface of YSZ due to the $Y_2O_3$ doping. Oxygen vacancies can be regarded as Lewis acid, which can promote the dissociation of lithium salts and fix the dissociated anion, thus facilitating the migration of lithium ions (Figure 16a).[179] Similarly, Sm doped $CeO_2$ is an appropriate modifier with an even higher concentration of oxygen vacancies. 10 wt% of the SDC/PVDF electrolyte could deliver an ionic conductivity of $9.09\times10^{-5}$ S cm$^{-1}$ at 30 °C.[180] There are also some special materials that are excellent at fixing the lithium salts dissociated anions. Halloysite nanotubes

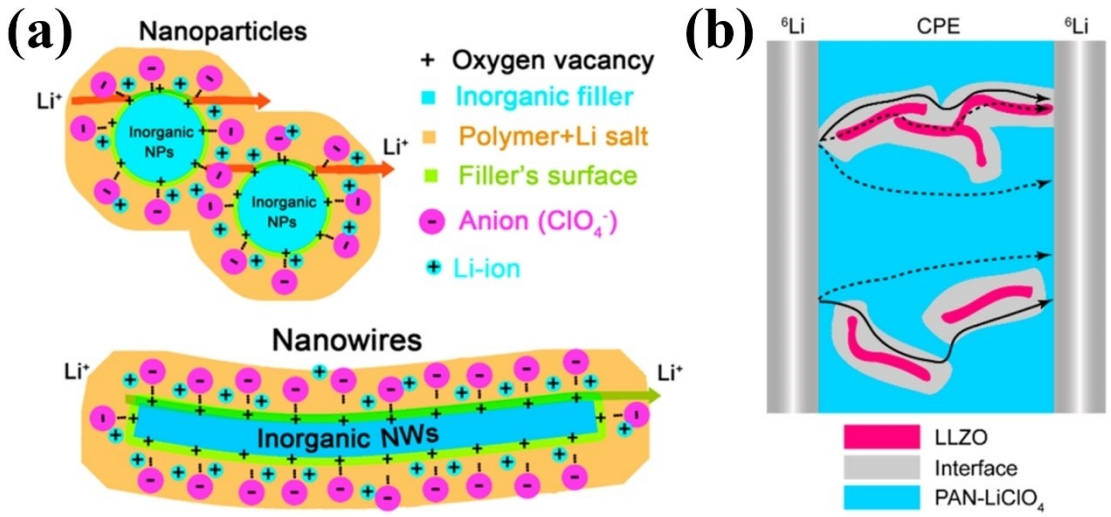


**Figure 16.** a) Schematic illustration for Li-ion transport in the composite polymer electrolytes with nanoparticle and nanowire modifiers. The positive-charged oxygen vacancies on the surfaces of the modifiers act as Lewis acid sites that can interact strongly with anions and release Li ions. A continuous fast conduction pathway can be seen for nanowires rather than nanoparticles[179] (reproduced with permission from Ref. [179], copyright (2016) American Chemical Society). b) Schematic showing possible Li + transport pathways in the composite polymer SSEs[181] (reproduced with permission from Ref. [181], copyright (2017) American Chemical Society).

(HNTs) are a complex ceramic modifier containing a variety of oxides, such as $SiO_2$, $Al_2O$, $Fe_2O$, $K_2O$, and $TiO_2$. With two oppositely charged surfaces, anions will be fixed on the positively charged inner surface, and lithium ions will be accommodated on the negatively charged outer surface. The absorbed lithium ions can then combine with the lone-pair electrons of the oxygen atom in PEO, which lead to PEO being wrapped around the HNTs surface to form a regular 3D channel for rapid lithium ion transport.

In many studies, the content of ceramic modifiers required to obtain the best performance differs to a large degree, such as 3% $TiO_2$ in PPC[159] and 40% LATP in PEO.[156] Yang et al. investigated the effect of the ceramic nanofiber modifier content on the lithium-ion transport mode using $^6$Li solid-state nuclear magnetic resonance (NMR). The results demonstrated lithium-ion transport along LLZO nanofibers in the electrolyte with 50 wt.% LLZO and along the PEO/LLZO interface in the electrolyte with 5 wt.% LLZO, as shown in Figure 16b.[181] This is due to too little LLZO in 5 wt.% LLZO-PEO electrolyte to form a continuous percolation network, so the lithium-ion conduction mode is the same as that of "ceramic-in-polymer" electrolyte. Correspondingly, 50 wt.% LLZO-PEO electrolyte is similar to a "polymer-in-ceramic" electrolyte, indicating that a continuous percolation network is necessary for lithium ions to pass through the bulk of the ceramic phase. A 50% additive is a sufficient amount to form the network. Considering that nanofibers can extend over long distances in a 1D direction, they could use fewer nanofibers and be easier to form network than nanoparticles.

## 3. Conclusions and Outlook

In this review, various ceramic electrolytes and polymer electrolytes are introduced, and their advantages and disadvantages discussed and compared. Then, the advantages and improvements provided by C/PCEs are introduced and summarized with a focus on the improvement of lithium-ion conductivity. As the performance improvement of C/PCEs is dependent on the morphology of the ceramic phase, C/PCEs are discussed in relation to the morphology of the ceramic phase. In summary, C/PCEs have the following characteristics:

Ceramic modifiers can improve ionic conductivity via two pathways: first, by enhancing the mobility of the chain segment by decreasing the polymer crystallinity; second by increasing the concentration of lithium ions and simultaneously fixing the anion through Lewis acid-base reactions. Generally, the C/PCEs design can facilitate improved polymer stability and enhance the electrochemical window, which is generally attributed to the interaction between the ceramic phase and polymer. In particular, 0D ceramic modifiers are most effective at reducing current density and concentration gradients because they are easiest to disperse evenly, which gives 0D ceramic modifiers excellent resistance to lithium dendrites. The 1D and 3D materials, especially the vertically arranged morphology, have much higher ionic conductivity than other composite forms by virtue of their ability to realize continuous lithium-ion transmission pathways. In addition, the defects of 1D or 3D ceramic modifier surfaces also provide a new path for lithium-ion transport. 2D materials have huge advantages due to their large effective area, but the extension direction of 2D materials can easily hinder lithium-ion transmission if it is not controlled.

In future studies, we believe that the following aspects are most critical:

doi.org/10.1002/batt.202000149


1) Further improvement of ionic conductivity. The ionic conductivity of C/PCE materials has reached the level of $10^{-5}$–$10^{-4}$ S cm$^{-1}$, but it is still far from the required $10^{-3}$–$10^{-2}$ S cm$^{-1}$.
2) As the ionic conductivity of C/PCEs is strictly limited by the conductivity of ceramic modifiers and polymer substrates, the development of new electrolytes with high ionic conductivity is a vital development direction.
3) Further research on the mechanism of lithium-ion transport in C/PCEs. Although there is a basic explanation, there are still different views and details of the mechanism remain unclear.
4) The development of more reliable test methods to elucidate the mechanism of lithium-ion transport and to provide guidance for material composites. Theoretical calculations can play an important role in the development of C/PCEs. First, they can provide directions for finding new electrolytes; second, they can establish a lithium-ion transport model, which can be confirmed with experimental results to clarify the mechanism of lithium-ion transport.
5) The structural design of the ceramic modifier in C/PCE should attract more attention. Compared with rough structures, well-designed and controlled structures can exert better results. Therefore, a manufacturing apparatus that can accurately control a structure such as 3D printing can be more widely used.

When designing C/PCEs, it is necessary to construct a channel for the rapid transfer of lithium ions or to guide lithium ions on shorter routes. Although current batteries assembled using C/PCEs show excellent properties, most studies report a small number of cycles and a low capacity retention rate. These issues highlight the need for better requirements for battery stability and interface improvement. In addition, just as simple polymer or ceramic electrolytes are difficult to meet all the requirements of solid electrolytes, the performance that C/PCE can specifically improve is also limited. Fortunately, different areas of lithium batteries have different needs. For example, a high-voltage-resistant electrolyte is required at the cathode, and a lithium dendritic electrolyte is required at the anode. Therefore, the combination of various electrolytes or composite electrolytes in different locations is a strategy worth considering and choosing.

## Acknowledgments

*The authors gratefully acknowledge financial support from the Australian Research Council Discovery Projects (DP160102627 and DP1701048343) of Australia and Shenzhen Peacock Plan of China (KQTD2016112915051055), and the 111 Project (D20015) of China Three Gorges University.*

## Conflict of Interest

The authors declare no conflict of interest.

**Keywords:** all-solid-state lithium batteries · solid-state electrolyte · ceramic/polymer composite electrolyte · ionic conductivity · interface engineering

[1] S. Chu, Y. Cui, N. Liu, *Nat. Mater.* **2017**, *16*, 16–22.
[2] A. Mauger, M. Armand, C. M. Julien, K. Zaghib, *J. Power Sources* **2017**, *353*, 333–342.
[3] J. M. Tarascon, M. Armand, *Nature* **2001**, *414*, 359–367.
[4] M. Armand, J. M. Tarascon, *Nature* **2008**, *451*, 652–657.
[5] Y. Cui, X. Zhou, W. Guo, Y. Liu, T. Li, Y. Fu, L. Zhu, *Batteries Supercaps* **2019**, *2*, 784–791.
[6] Y. S. Hong, C. Z. Zhao, Y. Xiao, R. Xu, J. J. Xu, J. Q. Huang, Q. Zhang, X. Yu, H. Li, *Batteries Supercaps* **2019**, *2*, 638–658.
[7] J. B. Goodenough, Y. Kim, *Chem. Mater.* **2010**, *22*, 587–603.
[8] D. Liu, Y. Tong, X. Yan, J. Liang, S. X. Dou, *Batteries Supercaps* **2019**, *2*, 743–765.
[9] M. Dirican, C. Yan, P. Zhu, X. Zhang, *Mater. Sci. Eng. R* **2019**, *136*, 27–46.
[10] Q. Zhou, J. Zhang, G. Cui, *Macromol. Mater. Eng.* **2018**, *303*, 1800337.
[11] H. Huo, Y. Chen, J. Luo, X. Yang, X. Guo, X. Sun, *Adv. Energy Mater.* **2019**, *9*, 1804004.
[12] M. Armand, *Solid State Ionics* **1983**, *9–10*, 745–754.
[13] N. J. Dudney, J. B. Bates, R. A. Zuhr, C. F. Luck, J. D. Robertson, *Solid State Ionics* **1992**, *53*, 655–661.
[14] D. E. Fenton, J. M. Parker, P. V. Wright, *Polymer* **1973**, *14*, 589–589.
[15] R. Gu, K. Yu, L. F. Wu, R. P. Ma, H. C. Sun, L. Jin, Y. L. Xu, Z. Xu, X. Y. Wei, *Ceram. Int.* **2019**, *45*, 8243–8247.
[16] C. L. Xu, W. Xiang, Z. G. Wu, Y. C. Li, Y. D. Xu, W. B. Hua, X. D. Guo, X. B. Zhang, B. H. Zhong, *J. Alloys Compd.* **2018**, *740*, 428–435.
[17] K. Yu, R. Gu, L. F. Wu, H. C. Sun, R. P. Ma, L. Jin, Y. L. Xu, Z. Xu, X. Y. Wei, *J. Alloys Compd.* **2018**, *739*, 892–896.
[18] Z. H. Zhang, S. J. Chen, J. Yang, G. Z. Liu, X. Y. Yao, P. Cui, X. X. Xu, *Electrochim. Acta* **2019**, *297*, 281–287.
[19] Y. Wang, B. N. Liu, G. Zhou, K. H. Nie, J. N. Zhang, X. Q. Yu, H. Li, *Chin. Phys. B* **2019**, *28*, 068202.
[20] S. V. Pershina, A. A. Pankratov, E. G. Vovkotrub, B. D. Antonov, *Ionics* **2019**, *25*, 4713–4725.
[21] L. H. Liu, L. H. Chu, B. Jiang, M. C. Li, *Solid State Ionics* **2019**, *331*, 89–95.
[22] X. W. Lai, G. R. Hu, Z. D. Peng, H. Tong, Y. Lu, Y. Z. Wang, X. Y. Qi, Z. C. Xue, Y. Huang, K. Du, Y. B. Cao, *J. Power Sources* **2019**, *431*, 144–152.
[23] X. G. Hao, Q. Zhao, S. M. Su, S. Q. Zhang, J. B. Ma, L. Shen, Q. P. Yu, L. Zhao, Y. Liu, F. Y. Kang, Y. B. He, *Adv. Energy Mater.* **2019**, *9*, 1901604.
[24] J. F. Bu, P. Leung, C. Huang, S. H. Lee, P. S. Grant, *J. Mater. Chem. A* **2019**, *7*, 19094–19103.
[25] X. Huang, Y. Lu, Z. Song, K. Rui, Q. S. Wang, T. P. Xiu, M. E. Badding, Z. Y. Wen, *Energy Storage Mater.* **2019**, *22*, 207–217.
[26] W. J. Lan, D. L. Lu, R. R. Zhao, H. Y. Chen, *Int. J. Electrochem. Sci.* **2019**, *14*, 9695–9703.
[27] A. J. Samson, K. Hofstetter, S. Bag, V. Thangadurai, *Energy Environ. Sci.* **2019**, *12*, 2957–2975.
[28] Y. L. Luo, Y. L. Zhang, Q. X. Zhang, Y. F. Zheng, H. Chen, L. C. Guo, *Ceram. Int.* **2019**, *45*, 17874–17883.
[29] T. Rosenthal, J. M. Weller, C. K. Chan, *Ind. Eng. Chem. Res.* **2019**, *58*, 17399–17405.
[30] T. Zhang, Z. Yang, H. L. Li, Q. C. Zhuang, Y. H. Cui, *Acta Chim. Sin.* **2019**, *77*, 525–532.
[31] Q. Zhang, J. Hu, Y. Chu, W. H. Wan, L. L. Zhao, Y. P. Zhu, *Mater. Lett.* **2019**, *248*, 153–156.
[32] E. Umeshbabu, B. Z. Zheng, J. P. Zhu, H. C. Wang, Y. X. Li, Y. Yang, *ACS Appl. Mater. Interfaces* **2019**, *11*, 18436–18447.
[33] R. Iwasaki, S. Hori, R. Kanno, T. Yajima, D. Hirai, Y. Kato, Z. Hiroi, *Chem. Mater.* **2019**, *31*, 3694–3699.
[34] S. H. Siyal, M. J. Li, H. Li, J. L. Lan, Y. H. Yu, X. P. Yang, *Appl. Surf. Sci.* **2019**, *494*, 1119–1126.
[35] V. Malinovschi, A. Marin, V. Andrei, E. Coaca, C. N. Mihailescu, C. P. Lungu, C. Radulescu, I. D. Dulama, *Surf. Coat. Technol.* **2019**, *375*, 621–636.
[36] Pritam, A. Arya, A. L. Sharma, *Ionics* **2019**, 1617–1632.
[37] D. E. Mathew, S. Gopi, M. Kathiresan, A. M. Stephan, S. Thomas, *Electrochim. Acta* **2019**, *319*, 189–200.
[38] L. Liu, L. Yang, M. Liu, X. Y. Wang, X. L. Li, D. S. Shao, K. L. Luo, Z. G. Luo, G. R. Chen, *J. Storage Mater.* **2019**, *25*, 100886.

[39] C. Wang, T. Wang, L. L. Wang, Z. L. Hu, Z. L. Cui, J. D. Li, S. M. Dong, X. H. Zhou, G. L. Cui, *Adv. Sci.* **2019**, *6*, 1901036.
[40] Q. Zhang, Y. Liu, J. Y. Ma, M. Zhang, X. Y. Ma, F. Chen, *Colloid. Surface. A.* **2019**, *580*, 123750.
[41] S. Sahoo, K. Krishnamoorthy, P. Pazhamalai, V. K. Mariappan, S. Manoharan, S. J. Kim, *J. Mater. Chem. A* **2019**, *7*, 21693–21703.
[42] J. L. Xu, Y. W. Liu, Q. Cao, B. Jing, X. Y. Wang, L. Tan, *J. Chem. Sci.* **2019**, *131*, 49.
[43] J. Lu, Y. C. Liu, P. H. Yao, Z. Y. Ding, Q. M. Tang, J. W. Wu, Z. R. Ye, K. Huang, X. J. Liu, *Chem. Eng. J.* **2019**, *367*, 230–238.
[44] P. Wang, J. C. Chai, Z. H. Zhang, H. R. Zhang, Y. Ma, G. J. Xu, H. P. Du, T. M. Liu, G. C. Li, G. L. Cui, *J. Mater. Chem. A* **2019**, *7*, 5295–5304.
[45] R. Manjuladevi, S. Selvasekarapandian, M. Thamilselvan, R. Mangalam, S. Monisha, P. C. Selvin, *Ionics* **2018**, *24*, 3493–3506.
[46] S. V. Ganesan, K. K. Mothilal, T. K. Ganesan, *Ionics* **2018**, *24*, 3845–3860.
[47] S. Kurapati, S. S. Gunturi, K. J. Nadella, H. Erothu, *Polym. Bull.* **2019**, *76*, 5463–5481.
[48] A. Hosseinioun, P. Nuernberg, M. Schoenhoff, D. Diddens, E. Paillard, *RSC Adv.* **2019**, *9*, 27574–27582.
[49] L. Long, S. Wang, M. Xiao, Y. Meng, *J. Mater. Chem. A* **2016**, *4*, 10038–10069.
[50] Q. Zhang, D. X. Cao, Y. Ma, A. Natan, P. Aurora, H. L. Zhu, *Adv. Mater.* **2019**, 1901131.
[51] A. Manthiram, X. W. Yu, S. F. Wang, *Nat. Rev. Mater.* **2017**, *2*, 16103.
[52] N. Zhao, W. Khokhar, Z. Bi, C. Shi, X. Guo, L. Z. Fan, C. W. Nan, *Joule* **2019**, *3*, 1190–1199.
[53] A. Kausar, *J. Plast. Film Sheeting* **2018**, *35*, 65–98.
[54] B. Commarieu, A. Paolella, J. C. Daigle, K. Zaghib, *Curr. Opin. Electrochem.* **2018**, *9*, 56–63.
[55] X. F. Yang, Q. Sun, C. T. Zhao, X. J. Gao, K. Adair, Y. Zhao, J. Luo, X. T. Lin, J. N. Liang, H. Huang, L. Zhang, S. G. Lu, R. Y. Li, X. L. Sun, *Energy Storage Mater.* **2019**, *22*, 194–199.
[56] L. J. Deiner, T. Jenkins, T. Howell, M. Rottmayer, *Adv. Eng. Mater.* **2019**, 1900952.
[57] J. L. Gai, F. R. Ma, Z. Q. Zhang, D. Y. Sun, Y. C. Jin, Y. J. Guo, W. Kim, *ACS Sustainable Chem. Eng.* **2019**, *7*, 15896–15903.
[58] C. D. Liu, G. Q. Cao, Z. H. Wu, J. H. Hu, H. Y. Wang, G. S. Shao, *ACS Appl. Mater. Interfaces* **2019**, *11*, 31991–31996.
[59] F. Jin, J. Li, C. J. Hu, H. C. Dong, P. Chen, Y. B. Shen, L. W. Chen, *Acta Phys. Chim. Sin.* **2019**, *35*, 1399–1403.
[60] X. L. Wang, X. J. Hao, Y. Xia, Y. F. Liang, X. H. Xia, J. P. Tu, *J. Membr. Sci.* **2019**, *582*, 37–47.
[61] Z. J. He, L. Chen, B. C. Zhang, Y. C. Liu, L. Z. Fan, *J. Power Sources* **2018**, *392*, 232–238.
[62] Z. J. He, L. Z. Fan, *Rare Met.* **2018**, *37*, 488–496.
[63] M. X. Jing, H. Yang, C. Han, F. Chen, W. Y. Yuan, B. W. Ju, F. Y. Tu, X. Q. Shen, S. B. Qin, *Ceram. Int.* **2019**, *45*, 18614–18622.
[64] H. Chen, M. X. Jing, C. Han, H. Yang, S. Hua, F. Chen, L. L. Chen, Z. X. Zhou, B. W. Ju, F. Y. Tu, X. Q. Shen, S. B. Qin, *Int. J. Energy Res.* **2019**, *43*, 5912–5921.
[65] Z. Xue, D. He, X. Xie, *J. Mater. Chem. A* **2015**, *3*, 19218–19253.
[66] J. Shin, *Electrochem. Commun.* **2003**, *5*, 1016–1020.
[67] J. M. Yu, C. Wang, S. H. Li, N. Liu, J. Zhu, Z. D. Lu, *Small* **2019**, 1902729.
[68] S. N. Banitaba, D. Semnani, E. Heydari-Soureshjani, B. Rezaei, A. A. Ensafi, *Mater. Res. Express* **2019**, *6*, 0850d6.
[69] P. Dhatarwal, S. Choudhary, R. J. Sengwa, *Compos. Commun.* **2018**, *10*, 11–17.
[70] J. Zheng, M. Tang, Y. Y. Hu, *Angew. Chem. Int. Ed. Engl.* **2016**, *55*, 12538–42.
[71] A. Bhide, K. Hariharan, *Eur. Polym. J.* **2007**, *43*, 4253–4270.
[72] C. Li, Y. Huang, X. Feng, Z. Zhang, P. Liu, *J. Membr. Sci.* **2019**, *587*, 117179.
[73] X. L. Wang, A. Mei, X. L. Li, Y. H. Lin, C. W. Nan, *J. Power Sources* **2007**, *171*, 913–916.
[74] Y. X. Li, J. A. Yerian, S. A. Khan, P. S. Fedkiw, *J. Power Sources* **2006**, *161*, 1288–1296.
[75] H. Pitawala, M. Dissanayake, V. A. Seneviratne, *Solid State Ionics* **2007**, *178*, 885–888.
[76] J. H. Choi, C. H. Lee, J. H. Yu, C. H. Doh, S. M. Lee, *J. Power Sources* **2015**, *274*, 458–463.
[77] L. P. Yue, J. Ma, J. J. Zhang, J. W. Zhao, S. M. Dong, Z. H. Liu, G. L. Cui, L. Q. Chen, *Energy Storage Mater.* **2016**, *5*, 139–164.
[78] W. Liu, N. Liu, J. Sun, P. C. Hsu, Y. Li, H. W. Lee, Y. Cui, *Nano Lett.* **2015**, *15*, 2740–2745.
[79] W. S. Jia, Z. L. Li, Z. R. Wu, L. P. Wang, B. Wu, Y. H. Wang, Y. Cao, J. Z. Li, *Solid State Ionics* **2018**, *315*, 7–13.
[80] J. Y. Song, Y. Y. Wang, C. C. Wan, *J. Power Sources* **1999**, *77*, 183–197.
[81] J. M. Tarascon, A. S. Gozdz, C. Schmutz, F. Shokoohi, P. C. Warren, *Solid State Ionics* **1996**, *86–8*, 49–54.
[82] R. Xu, X. Q. Zhang, X. B. Cheng, H. J. Peng, C. Z. Zhao, C. Yan, J. Q. Huang, *Adv. Funct. Mater.* **2018**, *28*, 1705838.
[83] J. Zhao, L. Liao, F. Shi, T. Lei, G. Chen, A. Pei, J. Sun, K. Yan, G. Zhou, J. Xie, C. Liu, Y. Li, Z. Liang, Z. Bao, Y. Cui, *J. Am. Chem. Soc.* **2017**, *139*, 11550–11558.
[84] A. Ali, M. Yahya, H. Bahron, R. Subban, M. K. Harun, I. Atan, *Mater. Lett.* **2007**, *61*, 2026–2029.
[85] W. Wieczorek, J. R. Stevens, *J. Phys. Chem. B* **1997**, *101*, 1529–1534.
[86] G. B. Appetecchi, F. Croce, B. Scrosati, *Electrochim. Acta* **1995**, *40*, 991–997.
[87] J. Bao, G. Shi, C. Tao, C. Wang, C. Zhu, L. Cheng, G. Qian, C. Chen, *J. Power Sources* **2018**, *389*, 84–92.
[88] J. J. Zhang, J. H. Zhao, L. P. Yue, Q. F. Wang, J. C. Chai, Z. H. Liu, X. H. Zhou, H. Li, Y. G. Guo, G. L. Cui, L. Q. Chen, *Adv. Energy Mater.* **2015**, *5*, 4940–4948.
[89] J. Lopez, D. G. Mackanic, Y. Cui, Z. Bao, *Nat. Rev. Mater.* **2019**, *4*, 312–330.
[90] H. I. Takehiko Takahashi, *Energy Convers.* **1971**, *11*, 105–111.
[91] H. X. Geng, J. L. Lan, A. Mel, Y. H. Lin, C. W. Nan, *Electrochim. Acta* **2011**, *56*, 3406–3414.
[92] Y. H. Cho, J. Wolfenstine, E. Rangasamy, H. Kim, H. Choe, J. Sakamoto, *J. Mater. Sci.* **2012**, *47*, 5970–5977.
[93] Z. F. Zheng, H. Z. Fang, Z. K. Liu, Y. Wang, *J. Electrochem. Soc.* **2015**, *162*, A244-A248.
[94] J. B. Goodenough, H. Y. P. Hong, J. A. Kafalas, *Mater. Res. Bull.* **1976**, *11*, 203–220.
[95] H. Aono, E. Sugimoto, Y. Sadaoka, N. Imanaka, G. Adachi, *J. Electrochem. Soc.* **1993**, *140*, 1827–1833.
[96] R. Inada, K. I. Ishida, M. Tojo, T. Okada, T. Tojo, Y. Sakurai, *Ceram. Int.* **2015**, *41*, 11136–11142.
[97] F. M. Du, N. Zhao, Y. Q. Li, C. Chen, Z. W. Liu, X. X. Guo, *J. Power Sources* **2015**, *300*, 24–28.
[98] X. G. Han, Y. H. Gong, K. Fu, X. F. He, G. T. Hitz, J. Q. Dai, A. Pearse, B. Y. Liu, H. Wang, G. Rublo, Y. F. Mo, V. Thangadurai, E. D. Wachsman, L. B. Hu, *Nat. Mater.* **2017**, *16*, 572–579.
[99] K. K. Fu, Y. H. Gong, B. Y. Liu, Y. Z. Zhu, S. M. Xu, Y. G. Yao, W. Luo, C. W. Wang, S. D. Lacey, J. Q. Dai, Y. N. Chen, Y. F. Mo, E. Wachsman, L. B. Hu, *Sci. Adv.* **2017**, *3*, e1601659.
[100] A. Sharafi, E. Kazyak, A. L. Davis, S. Yu, T. Thompson, D. J. Siegel, N. P. Dasgupta, J. Sakamoto, *Chem. Mater.* **2017**, *29*, 7961–7968.
[101] Y. Kato, S. Hori, T. Saito, K. Suzuki, M. Hirayama, A. Mitsui, M. Yonemura, H. Iba, R. Kanno, *Nat. Energy* **2016**, *1*, 16030.
[102] F. Han, Y. Zhu, X. He, Y. Mo, C. Wang, *Adv. Energy Mater.* **2016**, *6*, 1501590.
[103] F. Wu, W. Fitzhugh, L. Ye, J. Ning, X. Li, *Nat. Commun.* **2018**, *9*, 4037.
[104] S. Wenzel, S. Randau, T. Leichtwei, D. A. Weber, J. Sann, W. G. Zeier, J. Janek, *Chem. Mater.* **2016**, *28*, 2400–2407.
[105] H. Mehrer. (2010) Diffusion in Solids: Fundamentals, Methods, Materials, Diffusion-Controlled Processes, Springer Press.
[106] S. Stramare, V. Thangadurai, W. Weppner, *Chem. Mater.* **2003**, *15*, 3974–3990.
[107] M. Catti, *J. Phys. Chem. C* **2008**, *112*, 11068–11074.
[108] M. Weiss, D. A. Weber, A. Senyshyn, J. Janek, W. G. Zeier, *ACS Appl. Mater. Interfaces* **2018**, *10*, 10935–10944.
[109] V. Epp, Q. Ma, E. M. Hammer, F. Tietz, M. Wilkening, *Phys. Chem. Chem. Phys.* **2015**, *17*, 32115–21.
[110] F. A. Garcia Daza, M. R. Bonilla, A. Llordes, J. Carrasco, E. Akhmatskaya, *ACS Appl. Mater. Interfaces* **2019**, *11*, 753–765.
[111] S. Breuer, D. Prutsch, Q. Ma, V. Epp, F. Preishuber-Pflügl, F. Tietz, M. Wilkening, *J. Mater. Chem. A* **2015**, *3*, 21343–21350.
[112] Y. Zhang, F. Chen, J. Li, L. Zhang, J. Gu, D. Zhang, K. Saito, Q. Guo, P. Luo, S. Dong, *Electrochim. Acta* **2018**, *261*, 137–142.
[113] J. Zhang, H. Zhong, C. Zheng, Y. Xia, C. Liang, H. Huang, Y. Gan, X. Tao, W. Zhang, *J. Power Sources* **2018**, *391*, 73–79.
[114] J. Lou, G. Wang, Y. Xia, C. Liang, H. Huang, Y. Gan, X. Tao, J. Zhang, W. Zhang, *J. Power Sources* **2020**, *448*, 227440.
[115] J. Zhang, C. Zheng, J. Lou, Y. Xia, C. Liang, H. Huang, Y. Gan, X. Tao, W. Zhang, *J. Power Sources* **2019**, *412*, 78–85.
[116] C. Sun, Y. Ruan, W. Zha, W. Li, M. Cai, Z. Wen, *Mater. Horiz.* **2020**, *7*, 1667–1696.

[117] M. Du, K. Liao, Q. Lu, Z. Shao, *Energy Environ. Sci.* **2019**, *12*, 1780–1804.
[118] T. S. Wang, X. Liu, X. Zhao, P. He, C. W. Nan, L. Z. Fan, *Adv. Funct. Mater.* **2020**, *30*, 2000786.
[119] H. Xu, Y. Li, A. Zhou, N. Wu, S. Xin, Z. Li, J. B. Goodenough, *Nano Lett.* **2018**, *18*, 7414–7418.
[120] K. Liao, S. Wu, X. Mu, Q. Lu, M. Han, P. He, Z. Shao, H. Zhou, *Adv. Mater.* **2018**, e1705711.
[121] J. Fu, P. Yu, N. Zhang, G. Ren, S. Zheng, W. Huang, X. Long, H. Li, X. Liu, *Energy Environ. Sci.* **2019**, *12*, 1404–1412.
[122] M. Sumita, Y. Tanaka, M. Ikeda, T. Ohno, *J. Phys. Chem. C* **2016**, *120*, 13332–13339.
[123] J. Zhang, C. Zheng, L. Li, Y. Xia, H. Huang, Y. Gan, C. Liang, X. He, X. Tao, W. Zhang, *Adv. Energy Mater.* **2019**, *10*, 1903311.
[124] B. Zhang, L. Chen, J. Hu, Y. Liu, Y. Liu, Q. Feng, G. Zhu, L. Z. Fan, *J. Power Sources* **2019**, *442*, 227230.
[125] S. Zhang, Z. Li, Y. Guo, L. Cai, P. Manikandan, K. Zhao, Y. Li, V. G. Pol, *Chem. Eng. J.* **2020**, *400*,
[126] K. Zhu, Y. Liu, J. Liu, *RSC Adv.* **2014**, *4*, 42278–42284.
[127] J. Hu, W. Wang, H. Peng, M. Guo, Y. Feng, Z. Xue, Y. Ye, X. Xie, *Macromolecules* **2017**, *50*, 1970–1980.
[128] J. Li, C. Ma, M. Chi, C. Liang, N. J. Dudney, *Adv. Energy Mater.* **2015**, *5*, 1–13.
[129] R. Li, D. Wu, L. Yu, Y. Mei, L. Wang, H. Li, X. Hu, *Adv. Eng. Mater.* **2019**, *21*, 1900055.
[130] S. H. S. Cheng, K. Q. He, Y. Liu, J. W. Zha, M. Kamruzzaman, R. L. W. Ma, Z. M. Dang, R. K. Y. Li, C. Y. Chung, *Electrochim. Acta* **2017**, *253*, 430–438.
[131] Z. Huang, W. Pang, P. Liang, Z. Jin, N. Grundish, Y. Li, C. A. Wang, *J. Mater. Chem. A* **2019**, *7*, 16425–16436.
[132] Y. C. Jung, S. M. Lee, J. H. Choi, S. S. Jang, D. W. Kim, *J. Electrochem. Soc.* **2015**, *162*, A704-A710.
[133] D. H. Kuo, R. Lo, T. H. Hsueh, D. J. Jan, C. H. Su, *J. Power Sources* **2019**, *429*, 89–96.
[134] D. Lin, W. Liu, Y. Liu, H. R. Lee, P. C. Hsu, K. Liu, Y. Cui, *Nano Lett.* **2016**, *16*, 459–65.
[135] F. Ma, Z. Zhang, W. Yan, X. Ma, D. Sun, Y. Jin, X. Chen, K. He, *ACS Sustainable Chem. Eng.* **2019**, *7*, 4675–4683.
[136] J. Ou, G. Li, Z. Chen, *J. Electrochem. Soc.* **2019**, *166*, A1785-A1792.
[137] O. Sheng, C. Jin, J. Luo, H. Yuan, C. Fang, H. Huang, Y. Gan, J. Zhang, Y. Xia, C. Liang, W. Zhang, X. Tao, *J. Mater. Chem. A* **2017**, *5*, 12934–12942.
[138] J. Yang, X. Wang, G. Zhang, A. Ma, W. Chen, L. Shao, C. Shen, K. Xie, *Front. Chem.* **2019**, *7*, 388.
[139] Y. Zhao, C. Wu, G. Peng, X. Chen, X. Yao, Y. Bai, F. Wu, S. Chen, X. Xu, *J. Power Sources* **2016**, *301*, 47–53.
[140] J. Lu, Y. Liu, P. Yao, Z. Ding, Q. Tang, J. Wu, Z. Ye, K. Huang, X. Liu, *Chem. Eng. J.* **2019**, *367*, 230–238.
[141] J. Zhang, X. Zang, H. Wen, T. Dong, J. Chai, Y. Li, B. Chen, J. Zhao, S. Dong, J. Ma, L. Yue, Z. Liu, X. Guo, G. Cui, L. Chen, *J. Mater. Chem. A* **2017**, *5*, 4940–4948.
[142] X. Li, X. Wang, D. Shao, L. Liu, L. Yang, *J. Appl. Polym. Sci.* **2019**, *136*, 47498.
[143] X. Zhang, T. Liu, S. Zhang, X. Huang, B. Xu, Y. Lin, B. Xu, L. Li, C. W. Nan, Y. Shen, *J. Am. Chem. Soc.* **2017**, *139*, 13779–13785.
[144] Y. Sun, X. Zhan, J. Hu, Y. Wang, S. Gao, Y. Shen, Y. T. Cheng, *ACS Appl. Mater. Interfaces* **2019**, *11*, 12467–12475.
[145] J. Hu, P. He, B. Zhang, B. Wang, L. Z. Fan, *Energy Storage Mater.* **2020**, *26*, 283–289.
[146] K. He, C. Chen, R. Fan, C. Liu, C. Liao, Y. Xu, J. Tang, R. K. Y. Li, *Compos. Sci. Technol.* **2019**, *175*, 28–34.
[147] J. F. Wu, X. Guo, *J. Mater. Chem. A* **2019**, *7*, 2653–2659.
[148] M. Keller, G. B. Appetecchi, G. T. Kim, V. Sharova, M. Schneider, J. Schuhmacher, A. Roters, S. Passerini, *J. Power Sources* **2017**, *353*, 287–297.
[149] W. Zhang, J. Nie, F. Li, Z. L. Wang, C. Sun, *Nano Energy* **2018**, *45*, 413–419.
[150] N. Zhang, J. He, W. Han, Y. Wang, *J. Mater. Sci.* **2019**, *54*, 9603–9612.
[151] C. Wang, Y. Yang, X. Liu, H. Zhong, H. Xu, Z. Xu, H. Shao, F. Ding, *ACS Appl. Mater. Interfaces* **2017**, *9*, 13694–13702.
[152] H. Huo, B. Wu, T. Zhang, X. Zheng, L. Ge, T. Xu, X. Guo, X. Sun, *Energy Storage Mater.* **2019**, *18*, 59–67.
[153] J. Zhang, N. Zhao, M. Zhang, Y. Li, P. K. Chu, X. Guo, Z. Di, X. Wang, H. Li, *Nano Energy* **2016**, *28*, 447–454.
[154] C. Z. Zhao, X. Q. Zhang, X. B. Cheng, R. Zhang, R. Xu, P. Y. Chen, H. J. Peng, J. Q. Huang, Q. Zhang, *Proc. Natl. Acad. Sci. USA* **2017**, *114*, 11069–11074.
[155] J. Zagórski, J. M. López del Amo, M. J. Cordill, F. Aguesse, L. Buannic, A. Llordés, *ACS Appl. Energy Mater.* **2019**, *2*, 1734–1746.
[156] H. Zhai, P. Xu, M. Ning, Q. Cheng, J. Mandal, Y. Yang, *Nano Lett.* **2017**, *17*, 3182–3187.
[157] D. C. Lin, Y. Y. Liu, Y. Cui, *Nat. Nanotechnol.* **2017**, *12*, 194–206.
[158] K. Q. He, J. W. Zha, P. Du, S. H. Cheng, C. Liu, Z. M. Dang, R. K. Y. Li, *Dalton Trans.* **2019**, *48*, 3263–3269.
[159] S. Hua, M. X. Jing, C. Han, H. Yang, H. Chen, F. Chen, L. L. Chen, B. W. Ju, F. Y. Tu, X. Q. Shen, S. B. Qin, *Int. J. Energy Res.* **2019**, 7296–7305
[160] M. X. Jing, H. Yang, H. Chong, F. Chen, L. K. Zhang, X. Y. Hu, F. Y. Tu, X. Q. Shen, *J. Electrochem. Soc.* **2019**, *166*, A3019-A3027.
[161] K. Kimura, H. Matsumoto, J. Hassoun, S. Panero, B. Scrosati, Y. Tominaga, *Electrochim. Acta* **2015**, *175*, 134–140.
[162] K. K. Fu, Y. Gong, J. Dai, A. Gong, X. Han, Y. Yao, C. Wang, Y. Wang, Y. Chen, C. Yan, Y. Li, E. D. Wachsman, L. Hu, *Proc. Natl. Acad. Sci. USA* **2016**, *113*, 7094–9.
[163] S. Song, Y. Wu, W. Tang, F. Deng, J. Yao, Z. Liu, R. Hu, Alamusi, Z. Wen, L. Lu, N. Hu, *ACS Sustainable Chem. Eng.* **2019**, *7*, 7163–7170.
[164] Z. Sun, Y. Li, S. Zhang, L. Shi, H. Wu, H. Bu, S. Ding, *J. Mater. Chem. A* **2019**, *7*, 11069–11076.
[165] L. Chen, W. Li, L. Z. Fan, C. W. Nan, Q. Zhang, *Adv. Funct. Mater.* **2019**, *29*, 1970196.
[166] X. Wang, H. Zhai, B. Qie, Q. Cheng, A. Li, J. Borovilas, B. Xu, C. Shi, T. Jin, X. Liao, Y. Li, X. He, S. Du, Y. Fu, M. Dontigny, K. Zaghib, Y. Yang, *Nano Energy* **2019**, *60*, 205–212.
[167] T. Jiang, P. He, G. Wang, Y. Shen, C. W. Nan, L. Z. Fan, *Adv. Energy Mater.* **2020**, *10*, 2070052.
[168] J. Bae, Y. Li, J. Zhang, X. Zhou, F. Zhao, Y. Shi, J. B. Goodenough, G. Yu, *Angew. Chem. Int. Ed.* **2018**, *57*, 2096–2100.
[169] Z. Li, W. X. Sha, X. Guo, *ACS Appl. Mater. Interfaces* **2019**, *11*, 26920–26927.
[170] R. Li, S. Guo, L. Yu, L. Wang, D. Wu, Y. Li, X. Hu, *Adv. Mater. Interfaces* **2019**, *6*, 1900200.
[171] J. Shim, D. G. Kim, H. J. Kim, J. H. Lee, J. C. Lee, *ACS Appl. Mater. Interfaces* **2015**, *7*, 7690–701.
[172] D. Zhou, R. Liu, Y. B. He, F. Li, M. Liu, B. Li, Q. H. Yang, Q. Cai, F. Kang, *Adv. Energy Mater.* **2016**, *6*, 1502214.
[173] X. Zhang, J. Xie, F. Shi, D. Lin, Y. Liu, W. Liu, A. Pei, Y. Gong, H. Wang, K. Liu, Y. Xiang, Y. Cui, *Nano Lett.* **2018**, *18*, 3829–3838.
[174] L. Chen, Y. Li, S. P. Li, L. Z. Fan, C. W. Nan, J. B. Goodenough, *Nano Energy* **2018**, *46*, 176–184.
[175] M. Liu, Z. Cheng, S. Ganapathy, C. Wang, L. A. Haverkate, M. Tułodziecki, S. Unnikrishnan, M. Wagemaker, *ACS Energy Lett.* **2019**, *4*, 2336–2342.
[176] L. Zhu, P. Zhu, S. Yao, X. Shen, F. Tu, *Int. J. Energy Res.* **2019**, *43*, 4854–4866.
[177] P. Zhu, C. Yan, M. Dirican, J. Zhu, J. Zang, R. K. Selvan, C. C. Chung, H. Jia, Y. Li, Y. Kiyak, N. Wu, X. Zhang, *J. Mater. Chem. A* **2018**, *6*, 4279–4285.
[178] D. Li, L. Chen, T. Wang, L. Z. Fan, *ACS Appl. Mater. Interfaces* **2018**, *10*, 7069–7078.
[179] W. Liu, D. Lin, J. Sun, G. Zhou, Y. Cui, *ACS Nano* **2016**, *10*, 11407–11413.
[180] P. Lun, P. Liu, H. Lin, Z. Dai, Z. Zhang, D. Chen, *J. Membr. Sci.* **2019**, *580*, 92–100.
[181] T. Yang, J. Zheng, Q. Cheng, Y. Y. Hu, C. K. Chan, *ACS Appl. Mater. Interfaces* **2017**, *9*, 21773–21780.

Manuscript received: June 27, 2020
Revised manuscript received: July 27, 2020
Accepted manuscript online: August 5, 2020
Version of record online: September 18, 2020